State Estimation and Leakage Detection in Water Distribution Networks Using Constrained Zonotopes

Brenner S. Rego, Stelios G. Vrachimis, *Member, IEEE*, Marios M. Polycarpou, *Fellow, IEEE*, Guilherme V. Raffo, and Davide M. Raimondo, *Member, IEEE*

***Abstract*— State estimation in water distribution networks (WDNs) is a challenging task due to the scarcity of measurements and the presence of several modeling uncertainties. In the literature, pseudo-measurements are often required to obtain an observable model for state estimation, which are highly uncertain and mostly represented by bounded sets. This article proposes two new methods for set-based state estimation in WDNs, considering unknown-but-bounded measurement and model uncertainties to calculate bounds on the system states. A new interval method is proposed based on iterative computation of tight enclosures of the nonlinear head-loss functions, and bounding the solution of the algebraic equations using rescaling. This method, referred to as iterative slope approximation and rescaling (ISAR), is mildly more conservative than the iterative hydraulic interval state estimation (IHISE) method previously proposed by the authors, but significantly more computationally efficient. However, since intervals are not capable of capturing the dependencies between state variables, we propose the use of constrained zonotopes (CZs) as an additional step to both IHISE and ISAR. This yields two new algorithms for set-based state estimation of WDNs, capable of capturing the dependencies between hydraulic states, which result in sets with significantly smaller volumes than intervals. The benefits of CZs are also highlighted when the new enclosures are used for leakage detection. These provide higher leakage detection rates compared to intervals, as demonstrated in two case studies using benchmark WDNs.**

***Index Terms*— Constrained zonotopes (CZs), intervals, set-based computing, state estimation, water distribution networks (WDNs).**

This work was supported in part by the Italian Ministry for Research in the framework of the 2017 Program for Research Projects of National Interest (PRIN) under Grant 2017YKXYXJ, in part by the project INCT, the National Council for Scientific and Technological Development (CNPq), Brazil, under Grant 465755/2014-3, in part by the São Paulo Research Foundation (FAPESP), Brazil, under Grant 2014/50851-0, in part by the Brazilian agencies Coordination for Higher Education Staff Development (CAPES) under Grant 001 and Grant 88887.136349/2017-00, in part by the Minas Gerais Research Foundation (FAPEMIG) under Grant APQ-04483-18, in part by CNPq under Grant 315695/2020-0, in part by the European Union Horizon 2020 Program under Agreement 739551 (KIOS CoE), and in part by the Cyprus Research Promotion foundation program Restart 2010–2020 under Agreement Enterprises/0916/0023 (WaterAnalytics). Recommended by Associate Editor A. Marino. *(Corresponding author: Brenner S. Rego.)*

Brenner S. Rego and Guilherme V. Raffo are with the Graduate Program in Electrical Engineering and the Department of Electronics Engineering, Federal University of Minas Gerais, Belo Horizonte 31270-901, Brazil (e-mail: brennersr7@ufmg.br; raffo@ufmg.br).

Stelios G. Vrachimis and Marios M. Polycarpou are with the KIOS Research and Innovation Center of Excellence and the Department of Electrical and Computer Engineering, University of Cyprus, 1678 Nicosia, Cyprus (e-mail: vrachimis.stelios@ucy.ac.cy; mpolycar@ucy.ac.cy).

Davide M. Raimondo is with the Department of Electrical, Computer and Biomedical Engineering, University of Pavia, 27100 Pavia, Italy (e-mail: davide.raimondo@unipv.it).

Color versions of one or more figures in this article are available at https://doi.org/10.1109/TCST.2021.3130534.

Digital Object Identifier 10.1109/TCST.2021.3130534

I. Introduction

A WATER distribution network (WDN) is a system responsible for delivering water to consumers from water sources. The water industry is being modernized with the installation of sensors for monitoring WDNs, the use of supervisory control, and data acquisition (SCADA) systems. Integrated monitoring platforms can combine real-time sensor measurements with hydraulic models and geographical information systems. However, there is still the need for intelligent algorithms to process the acquired data and use them for important tasks such as state estimation. State estimation algorithms in WDNs infer the internal system states, such as water flows in pipes and pressures at nodes, given the available measurements. A complete view of system states supports the operators in decision-making and enables the early detection of hydraulic faults, such as leakages. It is estimated that every day more than 45 million m^3 of treated water is lost due to leakages in developing countries, which could have served 200 million consumers [1].

State estimation in WDNs is a challenging task due to the scarcity of measurements compared to the system size. Indeed, observability in WDNs is only achievable in networks of large pipes which bring water from sources to water utilities, called the transport networks [2]. In these networks, all the inflows and outflows are measured in real time, which is a sensor configuration that guarantees observability [3]. On transmission lines, it is possible to accurately locate leakages using pressure sensors, a transient pressure model, and a suitable methodology which considers modeling uncertainty [4], [5]. However, most pipe failures in WDNs occur in urban distribution networks in which transient models cannot be employed. This is because these typically complex networks contain pipe branches which disperse and dampen transient pressure waves [6]. Moreover, these networks may have hundreds of outlets that are not measured in real time. Water utilities typically sectorize urban networks into district metered areas (DMAs) and measure the inlet flow and pressure of each sub-network. A number of pressure sensors may exist in a DMA, typically used for pressure monitoring. To obtain hydraulic observability, groups of consumer nodes are modeled as a single outlet, and a high-resolution estimate of their consumption is determined using knowledge about population distributions and historical data [7]. However, these so-called pseudo-measurements of consumer demands are highly uncertain with no statistical characterization of their error to the true consumption. The best way to characterize their uncertainty is with the use of error bounds [8]. Moreover, WDN hydraulic models are often uncertain in their parameters, which clearly affects the quality of state estimation [9]. The most notable uncertain parameter is pipe roughness, which can be described as a measure of the impedance each pipe exhibits to the water flowing through it. This parameter cannot be determined experimentally for every pipe, thus an estimate based on the pipe material and age is usually adopted [10].

Standard state estimation techniques used in WDNs, such as Kalman filtering and weighted least-squares, require a measurement set that makes the system observable and the statistical characterization of sensor measurement error to give more weight to measurements originating from more accurate sensors [11], [12]. Then, using a mathematical model of the system, they produce an estimated point and covariance [13]. Given the nature of uncertainties in WDNs [4], [5], the approach of modeling uncertainties of input data as intervals has been proposed in [14] and [15]. This approach results in a set-based state estimate, which is often more useful to an operator than providing point and covariance estimates, due to the lack of statistical characterization of all the uncertainties involved.

Set-based state estimation methods are often called confidence limit analysis in the WDNs literature. The use of bounds for the representation of measurement uncertainty in WDNs was first introduced in [16], where it was incorporated to estimate interval enclosures of the states. A common way to obtain set-based states in WDNs using a nonlinear model is through Monte Carlo simulations (MCS) [17]. Nevertheless, this approach is computationally intensive, and the actual lower and upper bounds may not be reached even with a large number of simulations. On the other hand, bounds can be obtained without the need for extensive simulations using different methods such as the error maximization method [8], the ellipsoid method, and linear programming [14]. The bounds generated by these approaches are not guaranteed because of the linearization uncertainty introduced when using a linear approximation of the WDN hydraulic model, while they often neglect parameter uncertainty. An interesting approach when dealing with systems with bounded uncertainties is interval-based state estimation which has been studied extensively for linear systems [18], [19] and also used for specific classes of nonlinear systems (see, e.g. [15], [20]). In particular, a recent interval-based state estimation approach, specific for water systems, was proposed by Vrachimis *et al.* [15], in which an optimization-based method calculates interval enclosures of the states using a nonlinear hydraulic model and considering parameter, input, and measurement uncertainties. It is shown that the provided bounds on the states approximate closely those obtained by performing a large number of MCS. Such bounds can be used not only for state estimation, but also for leak detection [21].

In contrast to intervals, zonotopes are capable of capturing potential dependencies between state variables, while mitigating the wrapping effect inherent to state estimation methods based entirely on interval analysis [22]. During the last decades, zonotopes have been extensively used both in set-based state and parameter estimation of linear and nonlinear discrete-time systems [23]–[26], and also in active fault detection of linear discrete-time systems [27], [28] and linear descriptor systems [29]. Zonotopes have been used in parameter estimation and leak detection of WDNs in [30] and leak localization in [31]. Specifically, the latter requires linearization of the output equations, and conversions between the generator representation of zonotopes to polytopes either in half-space representation or in vertex representation. These conversions have combinatorial and exponential complexities, respectively, and can lead to dramatic computational times in higher dimensions [32].

Recently, constrained zonotopes (CZs) were proposed in [33] as an extension of zonotopes, in which additional linear equality constraints are taken into account, while maintaining the computational advantages of zonotopes. Besides the ability of capturing the dependency of state variables, these equalities allow CZs to describe asymmetric sets (in addition, general convex polytopes, if the complexity of the set is not limited) and also to incorporate equality constraints between the state variables into the mathematical description. CZs were used in set-based state estimation of linear discrete-time systems in [33], nonlinear discrete-time systems in [34] and [35], and active fault diagnosis of linear systems in [36]. In these works, the use of CZs demonstrated their ability to provide sharper enclosures than zonotopes for state estimation and also early fault diagnosis. Nevertheless, despite these advantages, to the best of the authors' knowledge, the properties of CZs have not been yet explored in methods for set-based state estimation and leak detection in WDNs.

This article proposes two new methods for set-based state estimation of WDNs based on CZs, considering unknown-but-bounded water demands and model parameters. Specifically, we first formulate the mathematical model of a WDN from the laws of conservation of energy and mass, which is later approximated by linear algebraic constraints. Accordingly, we propose an interval method based on iterative computation of tight enclosures of the water flows by bounding the solution of the linear algebraic equations using rescaling [33] and subsequently re-approximating the nonlinear equalities for the new flow bounds. This method is referred to as iterative slope approximation and rescaling (ISAR). The latter is mildly more conservative than the previous approach in [15] (IHISE) since the provided intervals are not optimal bounds. However, ISAR has a significant reduced computational burden due to requiring only algebraic operations (see Section III-D), which is favorable in realistic scenarios involving high-dimensional WDNs. Nevertheless, as mentioned before, intervals are not capable of capturing the dependencies between state variables. Therefore, in addition, we propose the use of CZs to obtain

TABLE I

NOTATION USED FOR WDN VARIABLES

Symbol	Description
h_i	Hydraulic head at node i
q_i	Water flow at link i
$\mathbf{B}$	Network incidence matrix
u_i	Effects of water reservoir and tank heads at link i
d_i	Water demand at node i
$f_i(\mathbf{q}_k)$	Head loss at link i
ℓ_i	Pressure-dependent leakage at node i
θ_i	Leak emitter coefficient at node i
ϕ	Leak exponent
η_i	Elevation of node i
α	Magnitude of the leakage
ρ	Average sum of nominal demands

tights bounds of the solution of the nonlinear algebraic equations, with linear approximation based on the final interval enclosures provided by both the approach described in [15] and ISAR. These two new algorithms for set-based state estimation of WDNs, with a fair trade-off between efficiency and accuracy, are both capable of capturing the dependencies between hydraulic heads and water flows. This result in sets with significantly smaller volumes than intervals and therefore with improved accuracy. The obtained enclosures are further used in passive leak detection of WDNs, in which, by being less conservative than intervals, allow a significant higher number of detections in several scenarios with different leak magnitudes. We investigate the key advantages of the proposed methods for set-based state estimation and leak detection in WDNs in numerical examples and also a realistic network, which highlights their improved efficiency and accuracy in comparison to intervals.

This manuscript is organized as follows. The topology of the WDNs considered in this work is described in Section II along with the corresponding mathematical formulation. Section III reviews the interval method proposed in [15], introduces the required mathematical background on CZs, describes a new interval method with reduced computational cost, and present the final enclosures described by CZs. The use of these enclosures for leakage detection in WDNs is discussed in Section IV. Numerical examples are presented in Section V, and Section VI concludes the article.

A. Notation

Table I summarizes the notation used for WDNs in this manuscript.

II. PROBLEM FORMULATION

The topology of a WDN is modeled by a directed graph denoted as $\mathcal{G} = (\mathcal{N}, \mathcal{L})$. Let $\mathcal{N} = \{1, \ldots, n_h\}$ be the set of all nodes, where $|\mathcal{N}| = n_h$ is the total number of nodes. These represent junctions of pipes, consumer water demand locations, reservoirs, and tanks. The hydraulic state associated with the nodes is the hydraulic head, indicated by $h_j,\ j \in \mathcal{N}$. The hydraulic head consists of the pressure at node j, whose minimum is the node elevation η_i with respect to a geodesic reference. Each node j is also associated with a water consumer demand at the node location, denoted by d_j. Demands drive the dynamics of a WDN and are an uncertain input to the system. Let $\mathcal{L} = \{1, \ldots, n_q\}$ be the set of links, where $|\mathcal{L}| = n_q$ is the total number of links. These represent network pipes, water pumps, and pipe valves. The hydraulic quantity associated with a link $i \in \mathcal{L}$ is the water flow, indicated by q_i. Moreover, u_i denotes the contribution of the level of water reservoirs and tanks to the ith link.

Consider a WDN with n_q links and n_h nodes, described by the nonlinear system of equations [10]

$$\mathbf{f}(\mathbf{q}_k) + \mathbf{B}\mathbf{h}_k = \mathbf{u}_k \tag{1a}$$

$$\mathbf{B}^T \mathbf{q}_k = \mathbf{d}_k \tag{1b}$$

where $k \geq 0$ denotes the time instant, $\mathbf{q}_k \in \mathbb{R}^{n_q}$ denote the water flows at the links, $\mathbf{h}_k \in \mathbb{R}^{n_h}$ denote the node heads, $\mathbf{B} \in \mathbb{R}^{n_q \times n_h}$ denotes the incidence matrix (whose elements are -1, 0, or 1 depending on the connectivity of nodes with links), $\mathbf{u}_k \in \mathbb{R}^{n_q}$ is the contribution of the level of water reservoirs and tanks, and $\mathbf{d}_k \in \mathbb{R}^{n_h}$ is the water demand by the consumers at the nodes. The nonlinear mapping $\mathbf{f}(\mathbf{q}_k) : \mathbb{R}^{n_q} \to \mathbb{R}^{n_q}$ denotes the head loss at the links, with its ith component $f_i(\mathbf{q}_k) \triangleq f_i(q_{i,k})$ being given by

$$f_i(q_{i,k}) = \begin{cases} r_i |q_{i,k}|^{(\nu-1)} q_{i,k}, & \text{if link } i \text{ is a pipe} \\ -\left(w_1 - w_2 q_{i,k}^{w_3}\right), & \text{if link } i \text{ is a pump} \end{cases} \tag{2}$$

with ν, w_1, w_2, $w_3 \in \mathbb{R}$ being known parameters derived from physical properties of their corresponding elements (i.e., pipes and pumps) [10]. On the other hand, the parameter $\mathbf{r} \in \mathbb{R}^{n_q}$ is assumed to be uncertain and to belong to a known interval R.

Given the known information on $\mathbf{u}_k$ and $\mathbf{d}_k$ at instant k, for $k \geq 0$, the objective of this work is to obtain tight bounds Q_k and H_k satisfying $\mathbf{q}_k \in Q_k$ and $\mathbf{h}_k \in H_k$. It is assumed that interval bounds U_k and D_k of $\mathbf{u}_k$ and $\mathbf{d}_k$, respectively, are known from historical data, such that $\mathbf{u}_k \in U_k$, $\mathbf{d}_k \in D_k$, for all $k \geq 0$. In addition, we assume that conservative interval bounds on the state $\mathbf{x}_k \triangleq (\mathbf{q}_k, \mathbf{h}_k)$ can be derived from physical constraints or available historical data.

III. SET-BASED STATE ESTIMATION OF WDNS

This section develops the proposed state estimation method for WDNs described by (1). Specifically, the method developed in [15], denoted by iterative hydraulic interval state estimation (IHISE), is summarized in Section III-A. Necessary concepts of CZs are presented in Section III-B. The proposed approximation for the nonlinear equalities (1) is described in Section III-C. The new interval method, denoted by ISAR, is presented in Section III-D, and, lastly, the proposal of using CZs as the final step for the interval methods is described in Section III-E.

A. Iterative Hydraulic Interval State Estimation (IHISE)

IHISE is a set-based state estimation methodology for WDNs first proposed in [2] and further developed in [15]. The methodology calculates bounds on the system states satisfying the nonlinear algebraic equations in (1) and given bounds on water demands and the model parameter $\mathbf{r}$. This is achieved using bounding linearization, a technique which restricts the nonlinearities within a convex set, thus converting the hydraulic equations in a form where state bounds can be calculated using convex optimization techniques. An iterative procedure minimizes the distance between upper and lower state bounds, by reducing the feasible set defined by bounding linearization at each step and converging to the tightest possible interval bounds. The IHISE is summarized in the following four steps.

1) Initial Bounds on the State Vector: The initial enclosure of the state $\mathbf{x}_k \in X_k$ is obtained by considering the physical properties of the network. The initial lower bounds $\mathbf{h}_k^{\mathrm{L}\,(0)}$ on the unknown head vector $\mathbf{h}_k$ are set as equal to the elevation of each node, while the initial upper bounds $\mathbf{h}_k^{\mathrm{U}\,(0)}$ are equal to the sum of reservoir and pump heads, which is physically the maximum head that any node in the WDN can achieve. We then note that each equation in (1a) is a function of only one $q_{i,k}$ and that the head-loss functions $f_i(q_{i,k})$ are inclusion isotonic [37] [meaning that $A \subseteq B \implies f(A) \subseteq f(B)$]. This property allows the calculation of initial bounds on the unknown water flows using interval arithmetic, given $[\mathbf{h}_k^{\mathrm{L}\,(0)}, \mathbf{h}_k^{\mathrm{U}\,(0)}]$ and the known bounds U_k of the reservoirs and tanks levels $\mathbf{u}_k$. This is done by rearranging (1a) with respect to q_i, $i \in \mathcal{L}$, and applying the inverse of f_i. The uncertain parameters $\boldsymbol{r}$ are handled as interval parameters. More details about this procedure are given in [15]. The initial bounds of the flow and head states are indicated by $Q_k^{(0)}$ and $H_k^{(0)}$, respectively.

2) Bounding Linearization of the Interval Nonlinear Terms: Let $m \geq 1$ denote the iteration index. This step encloses the uncertain nonlinear terms $\mathbf{f}(\mathbf{q}_k)$ by a convex set, for all[1] $\mathbf{q}_k \in Q_k^{(m-1)} = [\mathbf{q}_k^{\mathrm{L}}, \mathbf{q}_k^{\mathrm{U}}]$ and all the uncertain parameters $\mathbf{r} \in R$, using bounding linearization [15]. One way to achieve this is to enclose the image of each component of the nonlinear function $f_i(q_{i,k})$, for all $q_{i,k} \in [q_{i,k}^{\mathrm{L}}, q_{i,k}^{\mathrm{U}}]$ and $\mathbf{r} \in R$, between a lower line $\bar{f}_i^{\mathrm{L}}(q_{i,k})$ and an upper line $\bar{f}_i^{\mathrm{U}}(q_{i,k})$. These lines are defined as

$$\bar{f}_i^{\mathrm{L}}(q_{i,k}) = \lambda_i^{\mathrm{L}} q_{i,k} + \beta_i^{\mathrm{L}} \quad \forall i \in \mathcal{L} \tag{3a}$$

$$\bar{f}_i^{\mathrm{U}}(q_{i,k}) = \lambda_i^{\mathrm{U}} q_{i,k} + \beta_i^{\mathrm{U}} \quad \forall i \in \mathcal{L} \tag{3b}$$

with λ_i^{L}, λ_i^{U}, β_i^{L}, and β_i^{U} computed as explained in [15]. The corresponding convex enclosure is defined componentwise by the linear inequalities

$$\bar{f}_i^{\mathrm{L}}(q_{i,k}) \leq f_i(q_{i,k}) \leq \bar{f}_i^{\mathrm{U}}(q_{i,k}) \quad \forall q_{i,k} \in [q_{i,k}^{\mathrm{L}}, q_{i,k}^{\mathrm{U}}], i \in \mathcal{L}. \tag{4}$$

3) Solution of the Linear Interval System of Equations Using Linear Programming: The procedure described in Step 2 yields linear inequality constraints that allow one to replace $f_i(q_{i,k})$ in (1a) with new variables ζ_i, thus allowing the transformation of all the algebraic equations in (1) into a set of linear inequalities. Let $Q_k^{(m-1)} = [\mathbf{q}_k^{\mathrm{L}}, \mathbf{q}_k^{\mathrm{U}}]$, $H_k^{(m-1)} = [\mathbf{h}_k^{\mathrm{L}}, \mathbf{h}_k^{\mathrm{U}}]$, $U_k = [\mathbf{u}_k^{\mathrm{L}}, \mathbf{u}_k^{\mathrm{U}}]$, $D_k = [\mathbf{d}_k^{\mathrm{L}}, \mathbf{d}_k^{\mathrm{U}}]$, $\mathbf{\Lambda}^{\mathrm{L}} = \mathrm{diag}(\boldsymbol{\lambda}^{\mathrm{L}})$, and $\mathbf{\Lambda}^{\mathrm{U}} = \mathrm{diag}(\boldsymbol{\lambda}^{\mathrm{U}})$, with $\boldsymbol{\lambda}^{\mathrm{L}} = [\lambda_1^{\mathrm{L}} \cdots \lambda_{n_q}^{\mathrm{L}}]^T$, and $\boldsymbol{\lambda}^{\mathrm{U}} = [\lambda_1^{\mathrm{U}} \cdots \lambda_{n_q}^{\mathrm{U}}]^T$. An enclosure of the state set satisfying (1a) and (1b) can be obtained using the following linear inequalities:

$$\mathbf{u}_k^{\mathrm{L}} \leq \boldsymbol{\zeta} + \mathbf{B}\mathbf{h} \leq \mathbf{u}_k^{\mathrm{U}} \tag{5a}$$

$$\mathbf{d}_k^{\mathrm{L}} \leq \mathbf{B}^T \mathbf{q} \leq \mathbf{d}_k^{\mathrm{U}} \tag{5b}$$

$$\mathbf{\Lambda}^{\mathrm{L}}\mathbf{q} + \boldsymbol{\beta}^{\mathrm{L}} \leq \boldsymbol{\zeta} \leq \mathbf{\Lambda}^{\mathrm{U}}\mathbf{q} + \boldsymbol{\beta}^{\mathrm{U}} \tag{5c}$$

$$\mathbf{q}_k^{\mathrm{L}} \leq \mathbf{q} \leq \mathbf{q}_k^{\mathrm{U}} \tag{5d}$$

$$\mathbf{h}_k^{\mathrm{L}} \leq \mathbf{h} \leq \mathbf{h}_k^{\mathrm{U}} \tag{5e}$$

where $\boldsymbol{\beta}^{\mathrm{L}} = [\beta_1^{\mathrm{L}} \cdots \beta_{n_q}^{\mathrm{L}}]^T$ and $\boldsymbol{\beta}^{\mathrm{U}} = [\beta_1^{\mathrm{U}} \cdots \beta_{n_q}^{\mathrm{U}}]^T$. Note that all the interval sets have been replaced by their respective lower and upper bounds. Then, a total of $2(n_q + n_h)$ linear programs (LPs) are then formulated using (5a)–(5e), with decision variables given by $[\mathbf{q}^T \ \mathbf{h}^T \ \boldsymbol{\zeta}^T]^T = [\mathbf{x}^T \ \boldsymbol{\zeta}^T]^T$. Each pair of the following LPs provide the lower and upper bounds of the jth state variable x_j, with $j = 1, \ldots, n_h + n_q$:

$$\begin{cases} x_j^{\mathrm{L}} = \min\limits_{\mathbf{x},\boldsymbol{\zeta}} \ x_j \\ \qquad \text{s.t. (5a)–(5e)} \end{cases} \qquad \begin{cases} x_j^{\mathrm{U}} = \max\limits_{\mathbf{x},\boldsymbol{\zeta}} \ x_j \\ \qquad \text{s.t. (5a)–(5e).} \end{cases} \tag{6}$$

4) Iterative Solution of the Nonlinear System of Equations: The procedure in Step 3 leads to an interval solution of (1), denoted by $\tilde{X}_k^{(m)}$, which encloses the exact solution set denoted by X_k^*. An iterative method is then used to find a tight $X_k^{(m)}$ with respect to X_k^*, resulting from $X_k^{(m)} = X_k^{(m-1)} \cap \tilde{X}_k^{(m)}$, with $X^{(0)} = Q^{(0)} \times H^{(0)}$. At each iteration m, the previous refined set $X_k^{(m-1)}$ is used in the bounding linearization procedure of Step 2 to reduce the convex set defined by the inequalities (5). Step 3 is then repeated to produce a smaller set $\tilde{X}_k^{(m)}$. The iterations of the IHISE terminate when the relative change in the obtained enclosure $X_k^{(m)}$, given by the metric $e_k^{(m)}$, is smaller than a chosen tolerance value ε, that is, $e_k^{(m)} < \varepsilon$. This metric $e_k^{(m)}$ is given by

$$e_k^{(m)} \triangleq \left| \left(\mathbf{x}_k^{\mathrm{U}\,(m)} - \mathbf{x}_k^{\mathrm{L}\,(m)} \right) - \left(\mathbf{x}_k^{\mathrm{U}\,(m-1)} - \mathbf{x}_k^{\mathrm{L}\,(m-1)} \right) \right|_1. \tag{7}$$

The overall procedure of the IHISE methodology is described in Algorithm 1.

Algorithm 1 IHISE [15]

1: Assign initial bounds $H_k^{(0)}$ using physical constraints.
2: Compute initial bounds $Q_k^{(0)}$ according to Step 1.
3: Assign $X_k^{(0)} = Q_k^{(0)} \times H_k^{(0)}$, and $m = 1$.
4: Perform bounding linearization of $\mathbf{f}(\mathbf{q}_k)$ for $\mathbf{q}_k \in Q_k^{(m-1)}$.
5: Solve the pair of LPs (6) for $j = 1, \ldots, n_q + n_h$, and obtain $\tilde{X}_k^{(m)}$.
6: Assign $X_k^{(m)} = X_k^{(m-1)} \cap \tilde{X}_k^{(m)}$.
7: If $e^{(m)} < \varepsilon$, return $X_k^{(m)}$ and terminate. Otherwise, assign $m = m + 1$ and go to 4.

Note that each iteration in Algorithm 1 requires the solutions of $2(n_h + n_q)$ LPs. Assuming that the solution of each LP has the average complexity reported in [38], that is, it has average complexity of $O(N_d N_c^3)$, in which N_d and N_c are the number of decision variables and constraints, respectively, then the computational complexity of Algorithm 1 is $O(\kappa_m n^5)$, where $n = n_h + n_q$, and κ_m corresponds to the number of performed iterations.

[1]For notational simplicity, we omit the dependence on the iteration index m of some variables, such as most of the lower and upper bounds of intervals.

B. Constrained Zonotopes (CZs)

CZs, proposed in [33], are an extension of zonotopes that considers additional linear equality constraints. These equalities allow CZs to describe asymmetric convex polytopes, while maintaining most of the computational benefits of zonotopes.

Definition 1: A set $Z \subset \mathbb{R}^n$ is a CZ if there exists $(\mathbf{G}_z, \mathbf{c}_z, \mathbf{A}_z, \mathbf{b}_z) \in \mathbb{R}^{n\times n_g} \times \mathbb{R}^n \times \mathbb{R}^{n_c\times n_g} \times \mathbb{R}^{n_c}$ such that

$$Z = \{\mathbf{c}_z + \mathbf{G}_z\boldsymbol{\xi} : \|\boldsymbol{\xi}\|_\infty \leq 1, \mathbf{A}_z\boldsymbol{\xi} = \mathbf{b}_z\}. \tag{8}$$

Equation (8) is called constrained generator representation (CG-rep). Each column of $\mathbf{G}_z$ is a generator, $\mathbf{c}_z$ is the center, and $\mathbf{A}_z\boldsymbol{\xi} = \mathbf{b}_z$ are the constraints. We use the shorthand notation $Z = \{\mathbf{G}_z, \mathbf{c}_z, \mathbf{A}_z, \mathbf{b}_z\}$ for CZs, and $Z = \{\mathbf{G}_z, \mathbf{c}_z\}$ for zonotopes. Moreover, we denote by $B_\infty(\mathbf{A}_z, \mathbf{b}_z) = \{\boldsymbol{\xi} \in \mathbb{R}^{n_g} : \|\boldsymbol{\xi}\|_\infty \leq 1, \mathbf{A}_z\boldsymbol{\xi} = \mathbf{b}_z\}$ and $B_\infty^{n_g} = \{\boldsymbol{\xi} \in \mathbb{R}^{n_g} : \|\boldsymbol{\xi}\|_\infty \leq 1\}$, respectively, the n_g-dimensional constrained unitary hypercube and the unitary hypercube.[2]

A few set operations are often present in the computation of enclosures in set-based state estimation methods [33], [39]. Let $Z, W \subset \mathbb{R}^n$, $\mathbf{R} \in \mathbb{R}^{m\times n}$, and $Y \subset \mathbb{R}^m$. In addition, let the linear mapping, Minkowski sum, and generalized intersection, respectively, be defined by $\mathbf{R}Z \triangleq \{\mathbf{R}\mathbf{z} : \mathbf{z} \in Z\}$, $Z \oplus W \triangleq \{\mathbf{z} + \mathbf{w} : \mathbf{z} \in Z, \mathbf{w} \in W\}$, and $Z \cap_{\mathbf{R}} Y \triangleq \{\mathbf{z} \in Z : \mathbf{R}\mathbf{z} \in Y\}$. Using intervals, the Minkowski sum is exact, but $\mathbf{R}Z$ and $Z \cap_{\mathbf{R}} Y$ are conservative when $\mathbf{R}$ is not diagonal due to the wrapping effect. Moreover, all these operations can be computed exactly using convex polytopes, but require different representations whose conversion can be extremely expensive [40]. With zonotopes, both $\mathbf{R}Z$ and $Z \oplus W$ are trivial, but $Z \cap_{\mathbf{R}} Y$ is conservative and difficult to compute [24]. On the other hand, if the sets Z, W, and Y are CZs expressed in the CG-rep (8), these operations are computed trivially by [33]

$$\mathbf{R}Z = \{\mathbf{R}\mathbf{G}_z, \mathbf{R}\mathbf{c}_z, \mathbf{A}_z, \mathbf{b}_z\} \tag{9}$$

$$Z \oplus W = \left\{\begin{bmatrix}\mathbf{G}_z\ \mathbf{G}_w\end{bmatrix}, \mathbf{c}_z + \mathbf{c}_w, \begin{bmatrix}\mathbf{A}_z & \mathbf{0}\\ \mathbf{0} & \mathbf{A}_w\end{bmatrix}, \begin{bmatrix}\mathbf{b}_z\\ \mathbf{b}_w\end{bmatrix}\right\} \tag{10}$$

$$Z \cap_{\mathbf{R}} Y = \left\{\begin{bmatrix}\mathbf{G}_z\ \mathbf{0}\end{bmatrix}, \mathbf{c}_z, \begin{bmatrix}\mathbf{A}_z & \mathbf{0}\\ \mathbf{0} & \mathbf{A}_y\\ \mathbf{R}\mathbf{G}_z & -\mathbf{G}_y\end{bmatrix}, \begin{bmatrix}\mathbf{b}_z\\ \mathbf{b}_y\\ \mathbf{c}_y - \mathbf{R}\mathbf{c}_z\end{bmatrix}\right\}. \tag{11}$$

Equations (9)–(11) result only in a reasonable increase in the complexity of the CG-rep (8). As with zonotopes (and unlike polytopes), efficient methods for complexity reduction of CZs, that is, to enclose a CZ with another one with fewer generators and constraints, are available [33]. In addition, similar to the zonotope inclusion in [23], the following theorem provides a method to enclose, by a CZ, the product of an interval matrix and a CZ.

Theorem 1 ([35]): Let $X = \{\mathbf{G}, \mathbf{c}, \mathbf{A}, \mathbf{b}\} \subset \mathbb{R}^m$ be a CZ with n_g generators and n_c constraints, let $\mathbf{J} \in \mathbb{IR}^{n\times m}$ be an interval matrix, and consider the set $\mathbf{J}X \triangleq \{\hat{\mathbf{J}}\mathbf{x} : \hat{\mathbf{J}} \in \mathbf{J}, \mathbf{x} \in X\} \subset \mathbb{R}^n$. Let $\bar{\mathbf{G}} \in \mathbb{R}^{n\times \bar{n}_g}$ and $\bar{\mathbf{c}} \in \mathbb{R}^n$ satisfy $X \subseteq \{\bar{\mathbf{G}}, \bar{\mathbf{c}}\}$, and let $\mathbf{m} \in \mathbb{IR}^n$ be an interval vector such that $\mathbf{m} \supseteq (\mathbf{J} - \mathrm{mid}(\mathbf{J}))\bar{\mathbf{c}}$ and $\mathrm{mid}(\mathbf{m}) = \mathbf{0}$. Finally, let $\mathbf{P} \in \mathbb{R}^{n\times n}$ be a diagonal matrix defined by $P_{ii} = \mathrm{rad}(m_i) + \sum_{j=1}^{\bar{n}_g}\sum_{k=1}^{m} \mathrm{rad}(J_{ik})|\bar{G}_{kj}|$ for all $i = 1, 2, \ldots, n$. Then, $\mathbf{J}X$ is contained in the CZ-inclusion $\mathbf{J}X \subseteq \triangleleft(\mathbf{J}, X) \triangleq \mathrm{mid}(\mathbf{J})X \oplus \mathbf{P}B_\infty^n$.

[2]We drop the superscript n_g in $B_\infty(\mathbf{A}_z, \mathbf{b}_z)$ for the sake of simplicity.

C. Slope Approximation of the Nonlinear Equalities

Consider the initial bounds $Q_k^{(0)}$ and $H_k^{(0)}$ computed as in Section III-A1. The exact solution set of (1) for all $\mathbf{u}_k \in U_k$, $\mathbf{d}_k \in D_k$, is the set of all $\mathbf{q}_k \in Q_k^{(0)}$ and $\mathbf{h}_k \in H_k^{(0)}$ such that

$$\begin{aligned}\mathbf{f}(\mathbf{q}_k) + \mathbf{B}\mathbf{h}_k &\in U_k\\ \mathbf{B}^T\mathbf{q}_k &\in D_k.\end{aligned} \tag{12}$$

The following lemma presents an approximation of the nonlinear equalities (1) based on the bounding linearization procedure described in Section III-A2. This is referred to as slope approximation. Instead of the inequalities (5), Lemma 1 approximates (1) by set of linear algebraic equations.

Lemma 1: Let $\mathbf{q}_k \in [\mathbf{q}_k^{\mathrm{L}}, \mathbf{q}_k^{\mathrm{U}}] \subset \mathbb{IR}^{n_q}$, $\mathbf{h}_k \in \mathbb{R}^{n_h}$, and $(\mathbf{d}_k, \mathbf{u}_k) \in D_k \times U_k$, such that the nonlinear algebraic equations (1) hold. Then, there exists $\boldsymbol{\delta} \in B_\infty^{n_q}$, $\boldsymbol{\Delta} = \mathrm{diag}(\boldsymbol{\delta})$, $\boldsymbol{\Lambda}_+ \in \mathbb{R}^{n_q\times n_q}$, $\boldsymbol{\Lambda}_- \in \mathbb{R}^{n_q\times n_q}$, $\boldsymbol{\beta}_+ \in \mathbb{R}^{n_q}$, and $\boldsymbol{\beta}_- \in \mathbb{R}^{n_q}$ such that

$$\begin{cases}\boldsymbol{\Lambda}_+\mathbf{q}_k + \mathbf{B}\mathbf{h}_k = \mathbf{u}_k - \boldsymbol{\beta}_+ - \boldsymbol{\Delta}\big(\boldsymbol{\beta}_- + \boldsymbol{\Lambda}_-\mathbf{q}_k\big)\\ \mathbf{B}^T\mathbf{q}_k = \mathbf{d}_k.\end{cases} \tag{13}$$

Proof: For a given interval bound $[\mathbf{q}_k^{\mathrm{L}}, \mathbf{q}_k^{\mathrm{U}}]$, there exist real vectors $\boldsymbol{\lambda}^{\mathrm{L}}, \boldsymbol{\lambda}^{\mathrm{U}}, \boldsymbol{\beta}^{\mathrm{L}}, \boldsymbol{\beta}^{\mathrm{U}} \in \mathbb{R}^{n_q}$ such that $\lambda_i^{\mathrm{L}} q_i + \beta_i^{\mathrm{L}} \leq f_i(q_i) \leq \lambda_i^{\mathrm{U}} q_i + \beta_i^{\mathrm{U}}$ for all $i = 1, 2, \ldots, n_q$, and $\mathbf{q}_k \in [\mathbf{q}_k^{\mathrm{L}}, \mathbf{q}_k^{\mathrm{U}}]$ (see Section III-A). Therefore,

$$\begin{aligned}&\lambda_i^{\mathrm{L}} q_{i,k} + \beta_i^{\mathrm{L}} \leq f_i\big(q_{i,k}\big) \leq \lambda_i^{\mathrm{U}} q_{i,k} + \beta_i^{\mathrm{U}}\\ &\quad\iff f_i\big(q_{i,k}\big) \in \big[\lambda_i^{\mathrm{L}} q_{i,k} + \beta_i^{\mathrm{L}},\ \lambda_i^{\mathrm{U}} q_{i,k} + \beta_i^{\mathrm{U}}\big]\\ &\quad\iff f_i\big(q_{i,k}\big) \in \left(\frac{1}{2}\big(\beta_i^{\mathrm{U}} + \beta_i^{\mathrm{L}}\big) + \frac{1}{2}\big(\lambda_i^{\mathrm{U}} + \lambda_i^{\mathrm{L}}\big)q_{i,k}\right)\\ &\qquad\qquad \oplus\left(\frac{1}{2}\big(\beta_i^{\mathrm{U}} - \beta_i^{\mathrm{L}}\big) + \frac{1}{2}\big(\lambda_i^{\mathrm{U}} - \lambda_i^{\mathrm{L}}\big)q_{i,k}\right)B_\infty.\end{aligned}$$

Let $\boldsymbol{\Lambda}_+ = (1/2)\mathrm{diag}(\boldsymbol{\lambda}^{\mathrm{U}} + \boldsymbol{\lambda}^{\mathrm{L}})$, $\boldsymbol{\Lambda}_- = (1/2)\mathrm{diag}(\boldsymbol{\lambda}^{\mathrm{U}} - \boldsymbol{\lambda}^{\mathrm{L}})$, $\boldsymbol{\beta}_+ = (1/2)(\boldsymbol{\beta}^{\mathrm{U}} + \boldsymbol{\beta}^{\mathrm{L}})$, $\boldsymbol{\beta}_- = (1/2)(\boldsymbol{\beta}^{\mathrm{U}} - \boldsymbol{\beta}^{\mathrm{L}})$. Then, there exists $\boldsymbol{\delta} \in B_\infty^{n_q}$ such that

$$\mathbf{f}(\mathbf{q}_k) = \boldsymbol{\Lambda}_+\mathbf{q}_k + \boldsymbol{\beta}_+ + \boldsymbol{\Delta}\big(\boldsymbol{\beta}_- + \boldsymbol{\Lambda}_-\mathbf{q}_k\big) \tag{14}$$

where $\boldsymbol{\Delta} = \mathrm{diag}(\boldsymbol{\delta})$. Substituting (14) in the nonlinear equations (1) results in the system of equalities (13). ∎

D. Iterative Slope Approximation and Rescaling (ISAR)

In this section, we propose an iterative method to find interval bounds of the solution set of (13) with modest computational complexity, without requiring to solve LPs as in Algorithm 1. This method is based on iteratively enclosing the solution set of the slope approximation (13) by a constrained box in CG-rep, followed by the use of the rescaling procedure described in [33], to obtain sharp interval bounds of the solution. The resulting method is referred to as ISAR.

Let $s \geq 1$ denote the iteration index, and $\tilde{\mathbf{u}}_k \triangleq \mathbf{u}_k - \boldsymbol{\beta}_+ - \boldsymbol{\Delta}(\boldsymbol{\beta}_- + \boldsymbol{\Lambda}_-\mathbf{q}_k)$. Moreover, let $\tilde{U}_k^{(s)} \triangleq [\tilde{\mathbf{u}}_k^{\mathrm{L}}, \tilde{\mathbf{u}}_k^{\mathrm{U}}]$ be the interval obtained by evaluating the right-hand side of $\tilde{\mathbf{u}}_k$ for all $\mathbf{u}_k \in [\mathbf{u}_k^{\mathrm{L}}, \mathbf{u}_k^{\mathrm{U}}]$, $\mathbf{q}_k \in [\mathbf{q}_k^{\mathrm{L}}, \mathbf{q}_k^{\mathrm{U}}]$, and $\Delta_{ii} \in B_\infty$, using interval arithmetic. By defining the augmented vector $\tilde{\mathbf{p}}_k = (\mathbf{q}_k, \mathbf{h}_k, \tilde{\mathbf{u}}_k, \mathbf{d}_k) \in \tilde{P}_k^{(s)} \in \mathbb{IR}^{2n_q+2n_h}$, with

$$\tilde{P}_k^{(s)} = Q_k^{(s-1)} \times H_k^{(s-1)} \times \tilde{U}_k^{(s)} \times D_k \tag{15}$$

Algorithm 2 Rescaling [33]

1: Assign $E \leftarrow [-\mathbf{1}, \mathbf{1}] \subset \mathbb{R}^{n_g}, R \leftarrow (-\boldsymbol{\infty}, +\boldsymbol{\infty}) = \mathbb{R}^{n_g}$, $i = j = 1$.
2: If $A_{ij} \neq 0$, assign
$$R_j \leftarrow R_j \cap \Big(A_{ij}^{-1} b_i - \sum_{k \neq j} A_{ij}^{-1} A_{ik} E_k\Big),\ E_j \leftarrow E_j \cap R_j.$$
3: If $j < n_g$, assign $j \leftarrow j + 1$ and go to Step 2. Otherwise, if $j = n_g$ and $i < n_c$, assign $(i, j) \leftarrow (i + 1, 1)$ and go to Step 2. If $(i, j) = (n_c, n_g)$, assign $[\boldsymbol{\xi}^{\mathrm{L}}, \boldsymbol{\xi}^{\mathrm{U}}] \leftarrow E$ and terminate.

$$\tilde{\mathbf{B}} = \begin{bmatrix} \boldsymbol{\Lambda}_+ & \mathbf{B} & -\mathbf{I} & \mathbf{0} \\ \mathbf{B}^T & \mathbf{0} & \mathbf{0} & -\mathbf{I} \end{bmatrix}$$

the equalities (13) can be rewritten in the form $\tilde{\mathbf{B}}\tilde{\mathbf{p}}_k = \mathbf{0}$. In addition, the relation $\tilde{\mathbf{p}}_k \in \tilde{P}_k^{(s)}$ implies that there must exist a vector $\bar{\mathbf{p}} \in B_\infty^{2n_q + 2n_h}$ satisfying

$$\tilde{\mathbf{p}}_k = \mathrm{mid}\Big(\tilde{P}_k^{(s)}\Big) + \mathrm{diag}\Big(\mathrm{rad}\Big(\tilde{P}_k^{(s)}\Big)\Big)\bar{\mathbf{p}}. \tag{16}$$

Then, replacing (16) into the equalities $\tilde{\mathbf{B}}\tilde{\mathbf{p}}_k = \mathbf{0}$ results in $\tilde{\mathbf{B}}(\mathrm{mid}(\tilde{P}_k^{(s)}) + \mathrm{diag}(\mathrm{rad}(\tilde{P}_k^{(s)})\bar{\mathbf{p}})) = \mathbf{0}$, which, in turn, implies that $\tilde{\mathbf{B}}(\mathrm{diag}(\mathrm{rad}(\tilde{P}_k^{(s)})))\bar{\mathbf{p}} = -\tilde{\mathbf{B}}(\mathrm{mid}(\tilde{P}_k^{(s)}))$. Therefore, by defining the variables $\tilde{\mathbf{c}}_k = \mathrm{mid}(\tilde{P}_k^{(s)})$, $\tilde{\mathbf{G}}_k = \mathrm{diag}(\mathrm{rad}(\tilde{P}_k^{(s)}))$, $\tilde{\mathbf{A}} = \tilde{\mathbf{B}}(\mathrm{diag}(\mathrm{rad}(\tilde{P}_k^{(s)})))\bar{\mathbf{p}}$, and $\tilde{\mathbf{b}}_k = -\tilde{\mathbf{B}}(\mathrm{mid}(\tilde{P}_k^{(s)}))$, we have from (16) that the following relation holds:

$$\tilde{\mathbf{p}}_k \in \Big\{\tilde{\mathbf{c}}_k + \tilde{\mathbf{G}}_k\bar{\mathbf{p}} : \|\bar{\mathbf{p}}\|_\infty \leq 1, \tilde{\mathbf{A}}_k\bar{\mathbf{p}} = \tilde{\mathbf{b}}_k\Big\} \tag{17}$$

in which the right-hand side is a constrained box in CG-rep (note that $\tilde{\mathbf{G}}_k$ is diagonal). The rescaling procedure described in Property 1 is then applied to the right-hand side of (17) to obtain an approximated interval hull of the solution of $\tilde{\mathbf{A}}_k\bar{\mathbf{p}} = \tilde{\mathbf{b}}_k$ and, consequently, obtain a tight interval bound of $\tilde{\mathbf{p}}_k$.

Property 1 (Rescaling [33]): Let $Z = \{\mathbf{G}, \mathbf{c}, \mathbf{A}, \mathbf{b}\}$ be a CZ with $\mathbf{G} \in \mathbb{R}^{n \times n_g}$, $\mathbf{c} \in \mathbb{R}^n$, $\mathbf{A} \in \mathbb{R}^{n_c \times n_g}$, and $\mathbf{b} \in \mathbb{R}^{n_c}$. If $\boldsymbol{\xi}^{\mathrm{L}}$, $\boldsymbol{\xi}^{\mathrm{U}} \in \mathbb{R}^{n_g}$ satisfy $B_\infty(\mathbf{A}, \mathbf{b}) \subset [\boldsymbol{\xi}^{\mathrm{L}}, \boldsymbol{\xi}^{\mathrm{U}}] \subset [-\mathbf{1}, \mathbf{1}]$, then an equivalent CG-rep is

$$Z = \Big\{\mathbf{G}\mathrm{diag}\big(\boldsymbol{\xi}_{\mathrm{r}}\big), \mathbf{c} + \mathbf{G}\boldsymbol{\xi}_{\mathrm{m}}, \mathbf{A}\mathrm{diag}\big(\boldsymbol{\xi}_{\mathrm{r}}\big), \mathbf{b} - \mathbf{A}\boldsymbol{\xi}_{\mathrm{m}}\Big\} \tag{18}$$

where $\boldsymbol{\xi}_{\mathrm{m}} = (1/2)(\boldsymbol{\xi}^{\mathrm{L}} + \boldsymbol{\xi}^{\mathrm{U}})$ and $\boldsymbol{\xi}_{\mathrm{r}} = (1/2)(\boldsymbol{\xi}^{\mathrm{U}} - \boldsymbol{\xi}^{\mathrm{L}})$.

The rescaling procedure corresponds to the process of computing the smallest interval satisfying $B_\infty(\mathbf{A}, \mathbf{b}) \subset [\boldsymbol{\xi}^{\mathrm{L}}, \boldsymbol{\xi}^{\mathrm{U}}]$ and replacing $Z = \{\mathbf{G}, \mathbf{c}, \mathbf{A}, \mathbf{b}\}$ with the CG-rep (18). Sharp bounds can be obtained using the procedure described in Algorithm 2, which has been previously used in [33], whose complexity, in the case of (17), is $O(n^3)$ (assuming that every variable is proportional to the state dimension $n = n_q + n_h$). In addition, further accurate results can be obtained if the constraints $\mathbf{A}\boldsymbol{\xi} = \mathbf{b}$ are first preconditioned using Gauss–Jordan elimination.

The proposed ISAR algorithm involving the rescaling of (17) is illustrated in Algorithm 3. To obtain an interval $X_k^{(s)}$ to be used in the subsequent iteration, we neglect the equality constraints of the constrained box obtained in the rescaling procedure, which, in this case, is equivalent to computing its interval hull. Moreover, we use the metric $\varepsilon^{(s)}$ given by (7), with $m \triangleq s$, as stop criterion.[3] Since Algorithm 2 has complexity $O(n^3)$, we have that ISAR has complexity $O(\kappa_s n^3)$, with κ_s being the number of performed iterations by Algorithm 3, while IHISE has average complexity $O(\kappa_m n^5)$ (see Section III-A). These complexities are highlighted in Table II.

Algorithm 3 ISAR

1: Assign initial bounds $H_k^{(0)}$ using physical constraints.
2: Compute initial bounds $Q_k^{(0)}$ according to Section III-A.1.
3: Assign $X_k^{(0)} = Q_k^{(0)} \times H_k^{(0)}$, $s = 1$.
4: Compute the slope approximation (13) for $\mathbf{q}_k \in Q_k^{(s-1)}$.
5: Compute $\tilde{P}_k^{(s)}$ as in (15).
6: Rescale the constrained box in (17) using Property 1 and Algorithm 2.
7: Retrieve the interval $X_k^{(s)}$ from the resulting CG-rep by neglecting its equality constraints.
8: If $e^{(s)} < \varepsilon$, return $X_k^{(s)}$ and terminate. Otherwise, assign $s = s + 1$ and go to 4.

TABLE II
COMPUTATIONAL COMPLEXITIES OF IHISE AND ISAR

	IHISE	ISAR
Computational complexity	$O(\kappa_m n^5)$	$O(\kappa_s n^3)$

Remark 1: Step 7 in Algorithm 3 is equivalent to computing the interval hull of the set obtained by Property 1.

Remark 2: The interval provided by Algorithm 3 may not necessarily correspond to the interval hull of the solution of the linear algebraic equations in (13). However, these are still accurate enclosures of the solution set, as illustrated in Section V.

Remark 3: The ISAR method (Algorithm 3) is based on iterative computations of: 1) the slope approximation (13), followed by 2) the rescaling procedure (Algorithm 2). Hence, the convergence of Algorithm 2 guarantees that the approximation (13) will be smaller at each new iteration of Algorithm 3, thus consequently resulting in smaller inputs for the next computation of the rescaling procedure. Algorithm 2 is a particular case of the interval Gauss–Seidel iteration method presented in [41]. A convergence analysis of the latter can be found in the same reference.

E. Final Enclosure With CZs

The interval bounds obtained by ISAR can be tight, but due to the wrapping effect inherent to intervals, these are not able to capture the dependencies between all the state variables. Therefore, we consider a final step in the state estimation method using CZs to obtain a more accurate enclosure that takes into account these dependencies. The complete algorithm is denoted by ISAR-CZ. For the sake of completeness, we also consider applying this final step to the IHISE, with the corresponding algorithm denoted by IHISE-CZ.

[3] $\epsilon^{(s)} \neq \epsilon^{(s-1)}$ in general, therefore the notation $\epsilon^{(s)}$ is necessary.

Consider the slope approximation (13), the augmented vector $\mathbf{x}_k = (\mathbf{q}_k, \mathbf{h}_k)$ and the sets satisfying $(\mathbf{q}_k, \mathbf{h}_k) \in Q_k^{(\kappa_l)} \times H_k^{(\kappa_l)} = X_k^{(\kappa_l)}$, where $\kappa_l \triangleq \kappa_m$ or $\kappa_l \triangleq \kappa_s$ if the enclosure was obtained by IHISE or by ISAR, respectively. Let $\tilde{\mathbf{u}}_k = \mathbf{u}_k - \boldsymbol{\beta}_+ - \boldsymbol{\Delta}(\boldsymbol{\beta}_- + \boldsymbol{\Lambda}_- \mathbf{q}_k)$, with $\mathbf{u}_k \in U_k$. Then, it is true that $\tilde{\mathbf{u}}_k \in \check{U}_k$, where $\check{U}_k$ is a CZ given by

$$\check{U}_k \triangleq U_k \oplus \left(-\boldsymbol{\beta}_+\right) \oplus \triangleleft\left(\mathbf{D}, \boldsymbol{\beta}_- \oplus \boldsymbol{\Lambda}_- Q_k^{(\kappa_l)}\right)$$

with $\mathbf{D}$ being a diagonal interval matrix satisfying $D_{ii} = B_\infty^{n_q}$ for $i = 1, 2, \ldots, n_q$, such that $\boldsymbol{\Delta} \in \mathbf{D}$, and the operator $\triangleleft(\cdot, \cdot)$ is the CZ-inclusion defined in Theorem 1. The final enclosure used for state estimation is a CZ outer approximation of the solution set of (13) and is denoted by $\hat{X}_k$. For $\mathbf{u}_k \times \mathbf{d}_k \in U_k \times D_k$, this CZ is obtained by the generalized intersection

$$\hat{X}_k = \left\{\mathbf{x} \in X_k^{(\kappa_l)} : \mathbf{F}\mathbf{x} \in \tilde{U}_k \times D_k\right\} = X_k^{(\kappa_l)} \cap_{\mathbf{F}} \left(\check{U}_k \times D_k\right) \quad (19)$$

where $\mathbf{F} = \begin{bmatrix} \boldsymbol{\Lambda}_+ & \mathbf{B} \\ \mathbf{B}^T & \mathbf{0} \end{bmatrix}$.

In this article, we take advantage of the state coupling resulting from the nonlinear equality constraints (1), which are captured by the CZ[4] $\hat{X}_k$ given by (19). Moreover, since $Q_k^{(\kappa_l)}$, $H_k^{(\kappa_l)}$, D_k, and U_k are all intervals (hence have n_q, n_h, n_h, and n_q generators, respectively), the resulting enclosure $\hat{X}_k$ has $3n_q + 2n_h$ generators and $n_q + n_h$ constraints. Finally, to avoid numerical issues in $\hat{X}_k$ when one or both the sets U_k and D_k are degenerate, we add tolerance intervals $\{\tau_u, 0\}$ and $\{\tau_d, 0\}$ to each of the corresponding degenerate dimensions in U_k and D_k, respectively.

Remark 4: Although all the sets $Q_k^{(\kappa_l)}$, $H_k^{(\kappa_l)}$, U_k, and D_k are intervals (and therefore zonotopes), CZs are required to compute (19) because the generalized intersection (11) is difficult to enclose using zonotopes [24], which in addition results in conservative bounds.

Remark 5: In this work, the state estimation is assumed to be performed offline, using only the information obtained from physical constraints and historical data of the WDN. However, if measurements of $\mathbf{q}_k$ and $\mathbf{h}_k$ are available, these can be used to reduce the conservativeness of the initial bounds $Q_k^{(0)}$ and $H_k^{(0)}$ by intersecting them with the measurement bounds. This procedure can be done prior to computing the IHISE-CZ and ISAR-CZ and will be explored in future work.

IV. Passive Leak Detection in WDNs

Consider a WDN in the presence of leakages, with n_q links and n_h nodes, described by the nonlinear algebraic equation (1a), and

$$\mathbf{B}^T \mathbf{q}_k = \mathbf{d}_k + \boldsymbol{\ell}_k \quad (20)$$

where $\mathbf{q}_k \in \mathbb{R}^{n_q}$ are the water flows at the links, $\mathbf{B} \in \mathbb{R}^{n_q \times n_h}$ is the incidence matrix, and $\mathbf{d}_k \in \mathbb{R}^{n_h}$ is the water demand by the consumers at the nodes. In (20), $\boldsymbol{\ell}_k$ denotes the presence of pressure-dependent leakages modeled in this work at the nodes [42]. The purpose of leak detection is to check whether $\ell_{i,k} \neq 0$ for at least one node i.

Consider the output equation

$$\mathbf{y}_k = \mathbf{C}\mathbf{x}_k + \mathbf{v}_k \quad (21)$$

where $\mathbf{v}_k \in \mathbb{R}^{n_y}$ is the measurement uncertainty, and $Y_k \triangleq [\mathbf{y}_k^{\mathrm{L}}, \mathbf{y}_k^{\mathrm{U}}]$ is the obtained measurement interval, with $\mathrm{mid}(Y_k) = \mathbf{y}_k$. In this work, this condition can be verified conservatively[5] by checking if the following relation holds:

$$\mathbf{C}\hat{X}_k \cap Y_k = \emptyset \quad (22)$$

in which $\hat{X}_k$ is the set obtained by state estimation IHISE-CZ and ISAR-CZ without considering leakage. In the case of IHISE and ISAR, $\hat{X}_k$ is the interval provided by Algorithms 1 and 3, respectively.

Despite being conservative, the advantage in verifying if (22) holds is that no false positives can occur during leakage detection, given that the bounds on the uncertain parameters are valid, that is, $\mathbf{r} \in R$, $\mathbf{u}_k \in U_k$, and $\mathbf{d}_k \in D_k$, for all $k \geq 0$. The resulting CZ from the left-hand side in (22) can be computed using (9) and (11). Property 2 can be used to verify if this CZ is empty by solving an LP.

Property 2 ([33]): For every $Z = \{\mathbf{G}, \mathbf{c}, \mathbf{A}, \mathbf{b}\} \subset \mathbb{R}^n$, $Z \neq \emptyset$ iff $\min_{\boldsymbol{\xi}}\{\|\boldsymbol{\xi}\|_\infty : \mathbf{A}\boldsymbol{\xi} = \mathbf{b}\} \leq 1$.

V. Numerical Experiments

In this section, we show the efficiency and accuracy of the proposed CZ-based methods (IHISE-CZ and ISAR-CZ) for state estimation of WDNs. In addition, we show how these methods can be employed for leak detection (we consider scenarios where the leakage is present for the entire simulation) and compare their performance with the interval-based methods IHISE and ISAR. For these latter, the convergence tolerance (7) was set to $\varepsilon = 1$.

A. Uncertainty Modeling

For simulation purposes, all uncertainties in this work are assumed to have uniform distribution. This is because the most reliable representation for pseudo-measurement and pipe parameter uncertainties are with error bounds [8]. The parametric uncertainty $\mathbf{r} \in R$ is mostly attributed to unknown pipe roughness coefficients, which have typical values within a range depending on the pipe material [43]. Since these parameters remain relatively constant in practice, a calibration procedure can improve the estimation to a $\pm 5\%$ range of the estimated value for each pipe [44]. The measurement uncertainties are defined by the specifications of each type of sensor (e.g., pressure, flow). Typically, it is assumed that measurement uncertainties follow a normal distribution [45], while a uniform distribution can also be used based on the specification of sensor accuracy. Typical values for sensor accuracy are in the range of $\pm 2-5\%$ for flow sensors, while pressure sensors can have an accuracy as high as $\pm 0.3\%$ [46].

The most significant sources of uncertainties are the non-measured consumer demands. In this case, pseudo-measurements are used instead. These latter are essentially

[4]In case the complexity of the constrained zonotope (19) is very high, for computational purposes, the number of generators and constraints can be reduced using complexity reduction algorithms proposed in [33].

[5]Since $\hat{X}_k$ is computed conservatively, (22) $\implies$ $\ell_{i,k} \neq 0$ for at least one i, but the converse is not true in general.

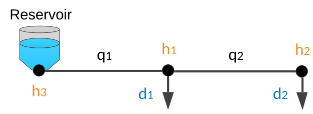

Fig. 1. Two-pipe network example.

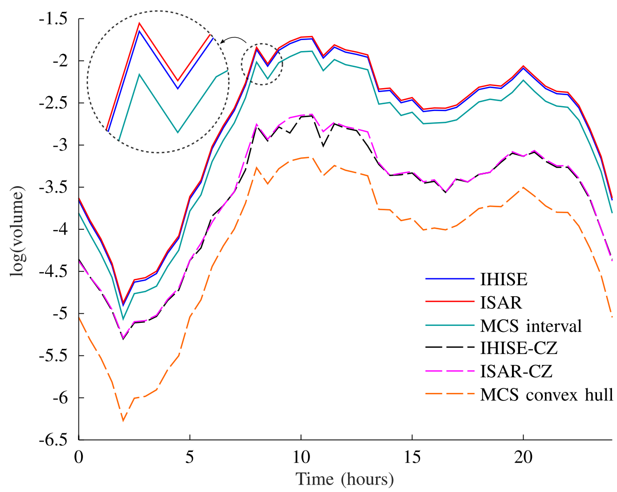

Fig. 2. Volumes of the sets $\hat{X}_k$ obtained using IHISE, IHISE-CZ, ISAR, ISAR-CZ, and also by the interval hull and convex hull of the trajectories resulting from 1000 Monte Carlo simulations (MCS) using EPANET for the two-pipe network.

short-term forecasts of consumption derived from historical data, such as low-resolution measurements of consumed water volume for billing purposes, as well as information about the consumer consumption patterns. There are various methods which can be used to estimate the demand [47], [48], with the study in [49] reporting that 95% of the forecast relative errors typically fall within the range of ±10% for 24-h forecasts. The demands in the transport network example (Section V-C), in which these are measured inflows of DMAs, are assumed to have ±5% uncertainty. In contrast, in the CY-DMA network example (Section V-D), which is a realistic DMA, demands have ±10% uncertainty due to the use of pseudo-measurements.

B. Two-Pipe Example

In this first example, we consider a network composed of three nodes and two pipes (see Fig. 1). A 24-h simulation was performed with EPANET [50], using conditions (water demands and reservoir levels) that vary every half of an hour. We consider that the physical parameters $\mathbf{r} \in R$ have uncertainty of 5%, the demands $\mathbf{d}_k \in D_k$ are measured with uncertainty of 5%, and the reservoir level $\mathbf{u}_k$ is precisely known. The tolerance values adopted in Section III-E are set to $\tau_u = 1.0 \times 10^{-4}$ m and $\tau_d = 1.0 \times 10^{-4}$ m^3/h.

Fig. 2 shows the volumes of the sets[6] $\hat{X}_k$, obtained using IHISE, ISAR, IHISE-CZ, and ISAR-CZ, for time $k \in [0, 24]$ in hours, in intervals of 30 min each. Fig. 2 also reports the volumes of "MCS interval" and "MCS convex hull." The former provides an interval approximation of the solution of

[6]For the sake of simplicity, in this section, we use the slight abuse of notation $\hat{X}_k \triangleq X_k^{(\kappa_I)}$ for the sets obtained using IHISE and ISAR.

TABLE III

AVERAGE EXECUTION TIMES AND NUMBER OF ITERATIONS PER TIME STEP IN THE TWO-PIPE EXAMPLE

	Average execution times (seconds)	Number of iterations (#)
IHISE	0.0243	2
ISAR	0.0118	3
IHISE-CZ	0.0286	2
ISAR-CZ	0.0167	3

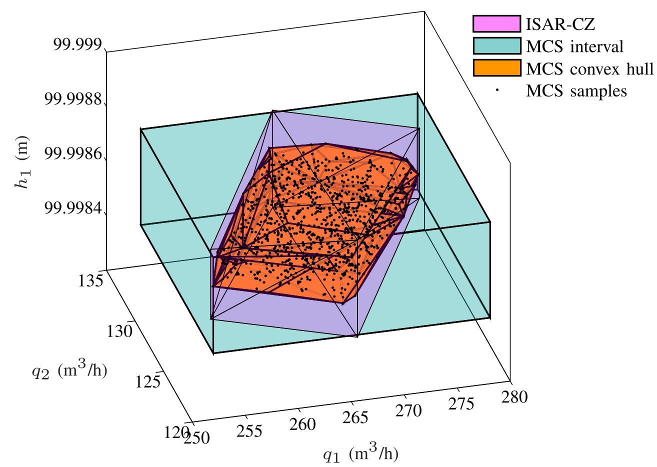

Fig. 3. Projections of $\hat{X}_0$ onto (q_1, q_2, h_1), obtained using ISAR-CZ, the intervals computed componentwise by maximum and minimum values obtained from 1000 MCS, as well as the convex hull and samples of the corresponding trajectories.

(1) obtained performing 1000 MCS considering parameters $\mathbf{r}$ and demands $\mathbf{d}_k$ drawn randomly from their corresponding uncertainty bounds. The latter is obtained by computing the convex hull of the same 1000 trajectories. Note that both results, being based on a finite number of samples, represent only an inner approximation of the solution of (1) but are useful as a reference for the set-based state estimation methods.

Table III shows the execution times of IHISE, ISAR, IHISE-CZ, and ISAR-CZ, averaged over the time horizon $k \in [0, 24]$, together with the number of iterations performed by the IHISE and ISAR for the given convergence tolerance ε. Note that the average execution time of ISAR is only 48.6% of the IHISE, even if a higher number of iterations is required. As expected, the volumes of the intervals/CZs provided by ISAR/ISAR-CZ are slightly bigger than the ones provided by IHISE/IHISE-CZ. Nevertheless, as shown in Fig. 2, this increase is reasonable, demonstrating that the drawback of using ISAR/ISAR-CZ is mild, while the advantage in terms of execution time is significant.

In addition, the volumes of both the outer convex approximations given by the CZs in IHISE-CZ and ISAR-CZ are smaller than the interval approximations provided by IHISE and ISAR (see Fig. 2), illustrating that both IHISE-CZ and ISAR-CZ can be significantly less conservative. Note that the volumes of the CZs are smaller even than MCS interval, demonstrating that CZs are indeed capable of capturing the existing coupling between the state variables. This effect is highlighted in Fig. 3, which shows the projections of $\hat{X}_0$ onto (q_1, q_2, h_1) obtained using ISAR-CZ, the sets corresponding

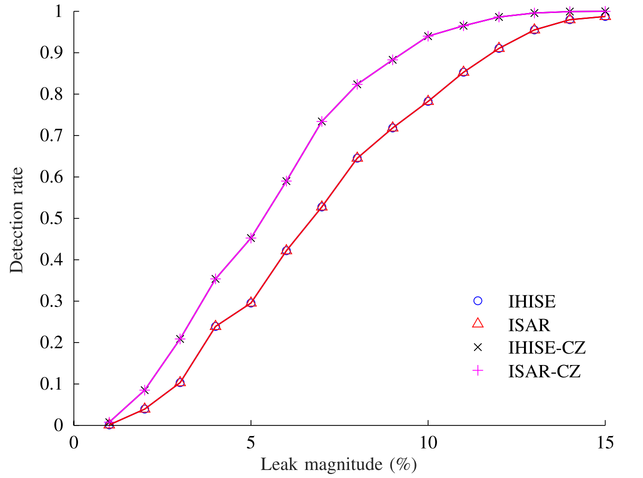

Fig. 4. Leak detection rate of the IHISE, ISAR, IHISE-CZ, and ISAR-CZ for the two-pipe network (leak at node 1), considering different leak magnitudes, averaged over 100 random simulations and the time interval $k \in [0, 24]$.

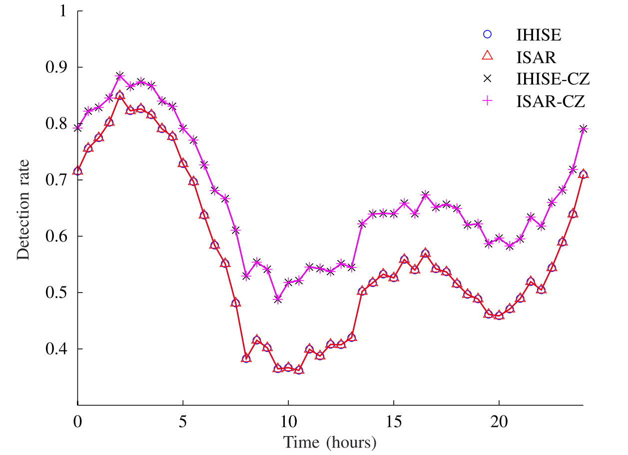

Fig. 5. Leak detection rate of the IHISE, ISAR, IHISE-CZ, and ISAR-CZ for the two-pipe network (leak at node 1) over time, averaged over 100 random simulations and the leak magnitudes in the interval [1, 15]%.

to MCS interval and MCS convex hull, and also the MCS trajectories.

In the following, we consider a scenario with the presence of a leakage at node 1. For illustration purposes, it is considered that all the water flows and hydraulic heads are measured, that is, $\mathbf{C}$ in (21) is the identity matrix. Specifically, the flows at pipes 1 and 2 and the heads at nodes 1 and 2 are all measured with uncertainty of 2%, that is, the measurement uncertainty in (21) is bounded by $\mathbf{v}_k \in V_k$, with $V_{k,i} = [-2\%|y_{k,i}|, 2\%|y_{k,i}|]$.

To generate a leakage at node i, this leakage is modeled by $\ell_{i,k} = \theta_i(h_{i,k} - \eta_i)^\phi$, where θ_i and ϕ denote the leak emitter coefficient and exponent, respectively [42], which are completely unknown to the fault detection methodologies. The leakage emitter exponent for all the leakages is given by $\phi = 0.5$. The emitter coefficient θ_i for a leakage at node i is given based on the average system inflow of the WDN (i.e., the sum of all nominal demands $d_{i,k}$ averaged over a given time horizon $k \in [0, N]$), denoted by ρ. Then, to generate $\ell_i \neq 0$, the emitter coefficient θ_i is set to

$$\theta_i = \frac{\alpha\rho}{\left(\bar{h}_i - \eta_i\right)^\phi}$$

where $\bar{h}_i$ is the nominal head of node i averaged over $k \in [0, N]$, and $\alpha \in [0, 100]\%$ is a parameter defining the magnitude of the leakage in comparison to the average total inflow ρ, referred as the leak magnitude.

Figs. 4 and 5 show the leak detection rate (a successful individual detection is denoted by 1, while 0 corresponds to the absence of detection), averaged over 100 MCS. The detection rates shown in Figs. 4 and 5 are further averaged over the leak magnitude range $\alpha = 1, 2, \ldots, 15\%$, and the time interval $k = 0, 1, \ldots, 24$ h, respectively. In this example, IHISE-CZ and IHISE provided exactly the same detection rates of ISAR-CZ and ISAR, respectively. Moreover, IHISE-CZ and ISAR-CZ provide up to about 20% more detections than IHISE and ISAR, demonstrating the improvements achieved in leak detection when using a set representation capable of taking into account the dependencies between water flows and hydraulic heads. This feature is highlighted in Fig. 6,

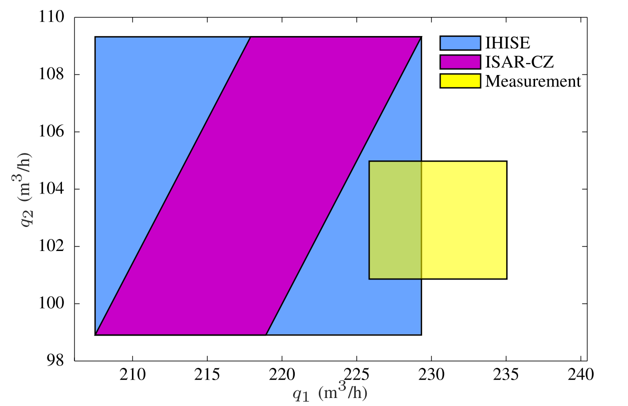

Fig. 6. Projection onto $\mathbf{q}_k \in \mathbb{R}^2$ of the sets $\hat{X}_k$ obtained using IHISE and ISAR-CZ, together with the measured flow interval for $\mathbf{q}_k$ at time $k = 2$ in one of the 100 random simulations considering leakage at node 1 of 4% of the average nominal inflow in the two-pipe example.

which shows the projection of the sets $\hat{X}_k$ provided by IHISE, ISAR-CZ, onto the water flows $(q_{1,k}, q_{2,k})$, as well as the corresponding projection of the measurement set Y_k, for time $k = 2$, in one of the 100 MCS considering leakage magnitude of 4%. This illustrates a case in which the leak has been successfully detected by the ISAR-CZ but not by the IHISE, which can be verified by the fact that the intersection of Y_k with the CZ provided by ISAR-CZ is empty, while the intersection with the interval provided by IHISE is not empty.

C. Transport Network

The second example considers the benchmark network "Net1," which is provided by EPANET, and is illustrated in Fig. 7. This network is composed of nine nodes and 13 pipes, and it is used here as an example of a real transport network. In the following, we consider that pipe parameters $\mathbf{r} \in R$ have uncertainty of 5%, the water demands at nodes $\mathbf{d}_k \in D_k$, which are inflows to DMAs, are measured with uncertainty of 5%, and the reservoir and tank levels $\mathbf{u}_k$ are precisely known. The tolerance values adopted in Section III-E are set to $\tau_u = 0.1$ m and $\tau_d = 0.1$ m^3/h.

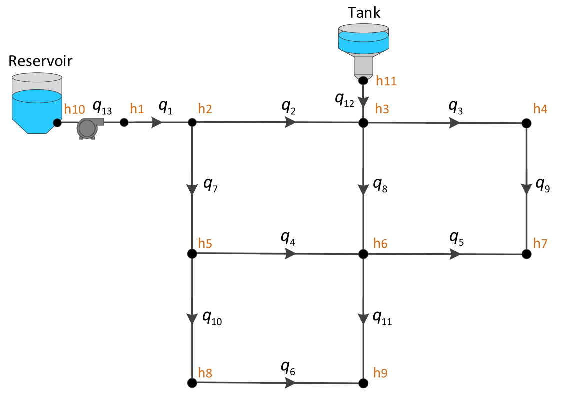

Fig. 7. Benchmark network "Net1," used here as an example of a transport network.

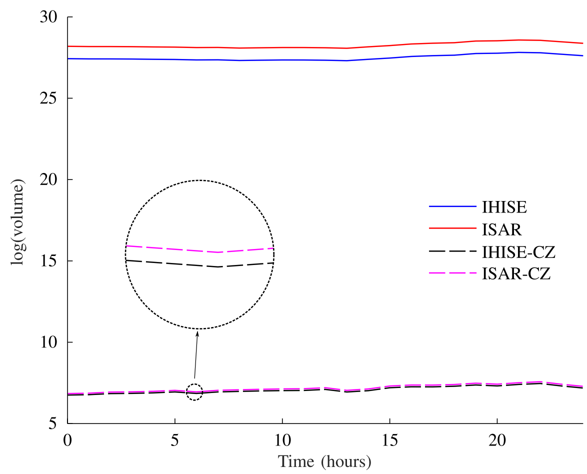

Fig. 8. Volumes of the sets $\hat{X}_k$ obtained using IHISE, IHISE-CZ, ISAR, and ISAR-CZ for the transport network "Net1."

Fig. 8 shows the volumes of the sets[7] $\hat{X}_k$ obtained using IHISE, ISAR, IHISE-CZ, and ISAR-CZ, for time $k \in [0, 24]$. As in the previous example, for this transport network, the volumes of the CZs generated by both IHISE-CZ and ISAR-CZ are significantly smaller than the volumes of the intervals provided by IHISE and ISAR, demonstrating that IHISE-CZ and ISAR-CZ can be significantly less conservative than IHISE and ISAR. Note also that the volumes of enclosures provided by IHISE-CZ and ISAR-CZ are very similar, showing that, also in this case, there is almost no drawback in terms of accuracy when using ISAR instead of IHISE. The corresponding execution times averaged over the time horizon $k \in [0, 24]$ are shown in Table IV, together with the number of iterations performed by the IHISE and ISAR. In this case, the average execution time of ISAR, which requires a higher number of iterations than IHISE, is only 7.4% of the time of IHISE.

We now assume that the flows at pipes 12 and 13, and the pressure at node 6 are measured, that is, $\mathbf{y}_k = (q_{k,12}, q_{k,13}, h_{k,6}) + \mathbf{v}_k$, where the measurement uncertainty is bounded by $\mathbf{v}_k \in V_k$, with $V_{k,i} = [-2\%|y_{k,i}|, 2\%|y_{k,i}|]$. Two leakage scenarios are considered, with the presence of leakage at node 8 and node 4, respectively.

[7]In this example, the fact that the sets $\hat{X}_k$ are in $\mathbb{R}^{22}$ results in intractable computational cost in obtaining the exact volumes of the CZs. Therefore, we show instead the volumes of the parallelotopes obtained by eliminating all the constraints in $\hat{X}_k$ followed by generator reduction, using the complexity reduction methods in [33] and [51], respectively. The volumes are computed using the formula in [52].

TABLE IV
AVERAGE EXECUTION TIMES AND NUMBER OF ITERATIONS PER TIME STEP FOR THE "NET1" TRANSPORT NETWORK

	Average execution times (seconds)	Number of iterations (#)
IHISE	0.6364	7–8
ISAR	0.0470	9
IHISE-CZ	0.6410	7–8
ISAR-CZ	0.0516	9

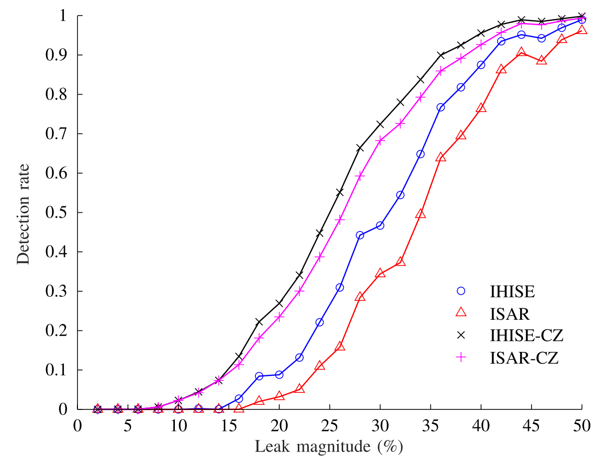

Fig. 9. Leak detection rate of the IHISE, ISAR, IHISE-CZ, and ISAR-CZ for the transport network "Net1" (leak at node 8), considering different leak magnitudes, averaged over 100 random simulations and the time interval $k \in [0, 24]$.

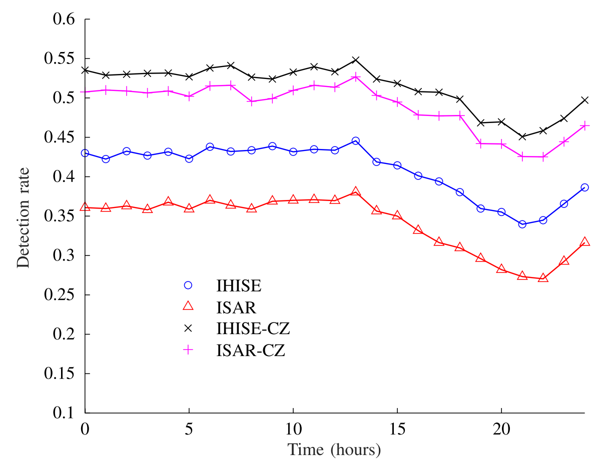

Fig. 10. Leak detection rate of the IHISE, ISAR, IHISE-CZ, and ISAR-CZ for the transport network "Net1" (leak at node 8) over time, averaged over 100 random simulations and the leak magnitudes in the interval $[2, 50]\%$.

Figs. 9 and 10 show the leak detection rate for the first scenario, averaged over 100 MCS, and further over the leak magnitude range $\alpha = 2, 4, \ldots, 50\%$, and the time interval $k = 0, 1, \ldots, 24$ h, respectively. In this example, IHISE-CZ provides up to about 20% more detections than IHISE, demonstrating once again the advantages of using CZs instead of intervals for leak detection of WDNs. In addition, Figs. 11 and 12 show the leak detection rate for the second scenario, averaged over 100 MCS, and further over the leak magnitude range $\alpha = 2, 4, \ldots, 50\%$, and the time interval

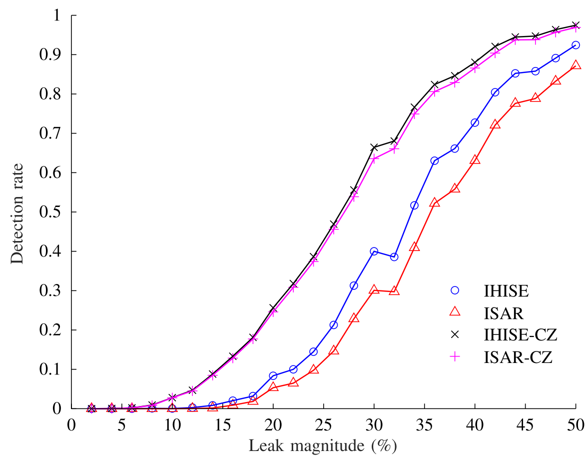

Fig. 11. Leak detection rate of the IHISE, ISAR, IHISE-CZ, and ISAR-CZ for the transport network "Net1" (leak at node 4), considering different leak magnitudes, averaged over 100 random simulations and the time interval $k \in [0, 24]$.

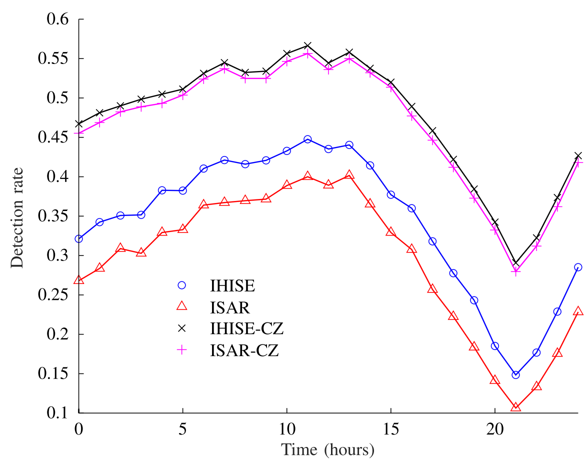

Fig. 12. Leak detection rate of the IHISE, ISAR, IHISE-CZ, and ISAR-CZ for the transport network "Net1" (leak at node 4) over time, averaged over 100 random simulations and the leak magnitudes in the interval [2, 50]%.

$k = 0, 1, \ldots, 24$ h, respectively. In the second scenario, once again the IHISE-CZ provides up to about 20% more detections than IHISE.

D. CY-DMA Network

The third example considers a realistic DMA network from a large water utility in Cyprus, denoted by "CY-DMA" [53]. The network is composed of 90 nodes and 130 pipes and is illustrated in Fig. 13. In this example, we consider that the physical parameters $\mathbf{r} \in R$ have uncertainty of 5%, the node demands $\mathbf{d}_k \in D_k$, which represent groups of residential consumers, are measured with uncertainty of 10%, and the reservoir level $\mathbf{u}_k$ is precisely known. The tolerance values adopted in Section III-E are set to $\tau_u = 1.0 \times 10^{-4}$ m and $\tau_d = 1.0 \times 10^{-4}$ m^3/h. Fig. 14 shows the volumes of the sets[8] $\hat{X}_k$ obtained using IHISE, ISAR, IHISE-CZ, and ISAR-CZ, for time $k \in [0, 24]$. For this realistic network, the volumes

[8]As in the previous example, for the CZs, we show the volumes of the parallelotopes obtained by eliminating all the constraints in $\hat{X}_k$ followed by generator reduction.

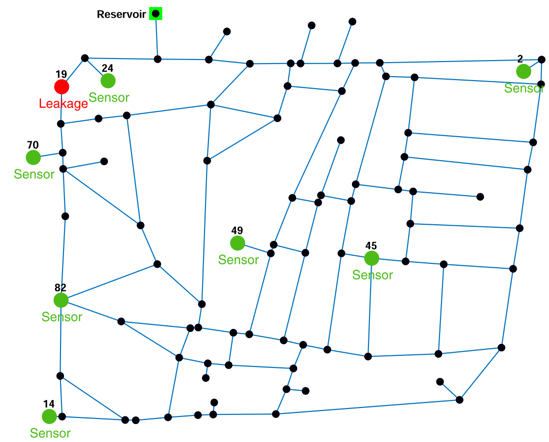

Fig. 13. "CY-DMA" network, a realistic example of a district metered area network.

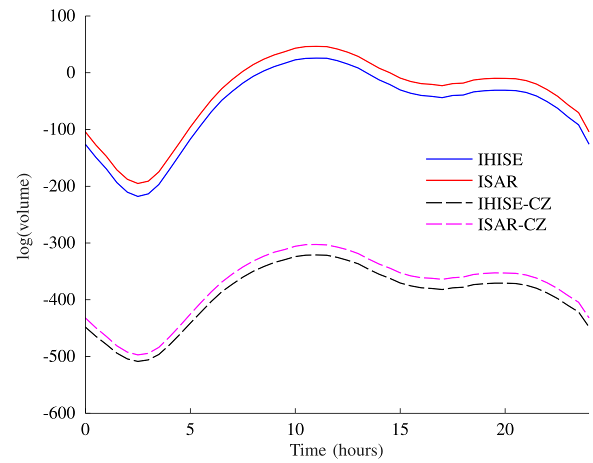

Fig. 14. Volumes of the sets $\hat{X}_k$ obtained using IHISE, IHISE-CZ, ISAR, and ISAR-CZ for the CY-DMA network.

TABLE V
AVERAGE EXECUTION TIMES AND NUMBER OF ITERATIONS PER TIME STEP FOR THE CY-DMA NETWORK

	Average execution times (seconds)	Number of iterations (#)
IHISE	54.5293	15–16
ISAR	5.8429	34–37
IHISE-CZ	54.5549	15–16
ISAR-CZ	5.8670	34–37

of the CZs generated by both IHISE-CZ and ISAR-CZ are, once again, significantly smaller than the bounds provided by IHISE and ISAR. Note that, due to the dimensionality of the CY-DMA network, considering, for instance, a rectangular set with uncertainty of 0.1 would result in $\log(\text{volume}) = -220$. Taking this into account, in particular, the IHISE-CZ is capable of providing sets with about $\log(\text{volume}) = -500$. The corresponding execution times averaged over $k \in [0, 24]$ are shown in Table V, together with the number of iterations performed by the IHISE and ISAR. Note that the average execution time of ISAR, which requires a higher number of iterations than IHISE, is only 10.7% of the time of IHISE.

We now consider a leakage scenario, with the presence of leakage at node 19. It is considered that the inlet flow (pipe 14) and pressure (node "Reservoir") are measured. Moreover, it is considered that the water utility has installed pressure sensors

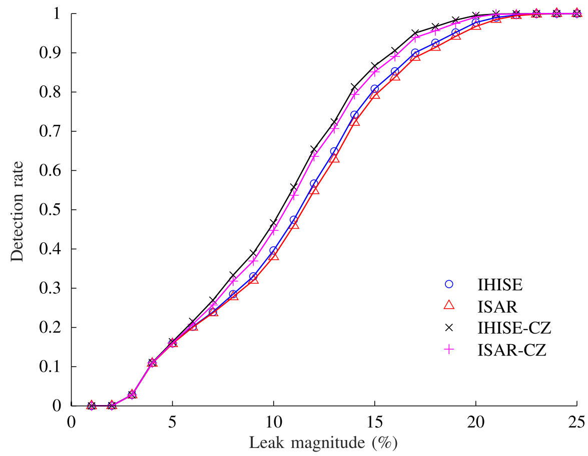

Fig. 15. Leak detection rate of the IHISE, ISAR, IHISE-CZ, and ISAR-CZ for the CY-DMA network (leak at node 19), considering seven pressure sensors, different leak magnitudes, averaged over 100 random simulations and the time interval $k \in [0, 24]$.

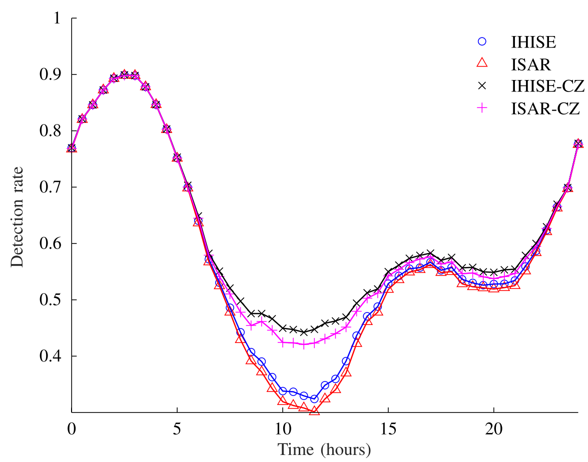

Fig. 16. Leak detection rate of the IHISE, ISAR, IHISE-CZ, and ISAR-CZ for the CY-DMA network (leak at node 19) over time, considering seven pressure sensors, averaged over 100 random simulations and the leak magnitudes in the interval $[1, 25]\%$.

at nodes 2, 14, 24, 45, 49, 70, and 82, with a total of seven pressure sensors. The sensors' positions were chosen using a sensor placement procedure which calculates the sensitivity matrix of the WDN and, using a heuristic optimization approach, computes the sensor locations that maximize the collective sensitivity of all sensors to all possible leakages [54]. The measured flows and pressures have uncertainties of 2% and 0.35%, respectively.

Figs. 15 and 16 show the leak detection rate, averaged over 100 MCS, and further over the leak magnitude range $\alpha = 1, 2, \ldots, 25\%$, and the time interval $k = 0, 1, \ldots, 24$ h, respectively. In this scenario, IHISE-CZ could provide up to about 10% more detections than IHISE. In this scenario, it is interesting to note that the advantage of using CZs instead of intervals is more expressive for leakage detection during midday (12:00–13:00) rather than night hours (3:00–4:00). This realistic network uses typical residential demand patterns with peak during midday and minimum flow demands during night. The high-pressure conditions resulting from the low demands during night hours cause the leakage magnitude to increase, which makes the leakage more evident to the leakage detection methodologies. The ability of CZs to consider the dependencies between state variables results in the interesting capability of providing higher detection rates even at peak demand hours, which reduces the time of detection and water loss. Finally, a few different leakage scenarios have been simulated taking into account several additional pressure sensors in the CY-DMA. However, due to the optimal placement of pressure sensors, the improvement in leak detection of all the methods was mild, which do not cope with the cost of placing additional sensors in a realistic network, and for this reason were not reported.

E. Practical Aspects and Limitations

The main challenge when practically applying the proposed model-based methodology is the construction of a system model which includes realistic uncertainties in network parameters and water demands. The specificity of fault-diagnosis depends on the inclusion of the true parameter values in the constructed uncertainty sets, while the sensitivity depends on how conservative the chosen uncertainty bounds are.

Model parameters such as pipe characteristics are typically modeled more accurately and affect the calculated state set less than water demands, which is the greatest source of uncertainty in these systems due to the lack of measurements in DMAs. However, using a suitable demand estimator to produce pseudo-measurements, demand uncertainty can remain within approximately $\pm 10\%$ of the estimated value, which leads to acceptable fault-diagnosis sensitivity when using the proposed methodology, as shown in the case studies of this work. A suitable demand estimator may use many sources of available information such as stochastic predictions of water usage at a residential level, building areas and population densities from governmental open data, as well as historical low-resolution measurements gathered for billing purposes.

The proposed leakage detection methodology can detect additional events in the system which may not correspond to leakages, provided that they cause changes to non-monitored demand locations or change hydraulic properties of the network. For example, the use of fire hydrants by the fire department will result to a fault signature similar to that of a leakage which may be detected by the proposed methodology. Moreover, changes in the network topology, such as the closing of a valve, will also be detected as a fault since the model used by the methodology does not contain this change. Finally, abnormal demand consumption in locations where pseudo-measurements are used will also result in an alert. In these cases, it is important for the operators to inform and update the model used by the proposed methodology, since most of these changes may be known *a priori* or can be interpreted by the operators when these are detected. At the current stage, the proposed methodology did not focus on distinguishing between the aforementioned events and automatically update the model used.

VI. Conclusion and Future Work

This article proposed two new methods for set-based state estimation of WDN based on CZs, namely IHISE-CZ and ISAR-CZ. With respect to interval-based methods, CZ-based ones are able to capture the dependencies between hydraulic states, resulting in sets with significantly smaller volumes. The benefits of IHISE-CZ and ISAR-CZ were also demonstrated for leakage detection in WDNs. In particular, the simulation results on a benchmark transport network and on a realistic DMA network show an increase in detection rates of up to 20% when using the proposed methods, while also requiring significantly less computational resources to compute the enclosures. Moreover, it is observed that the proposed methods perform well during peak demand hours, thus reducing significantly the time-to-detection and the cost of water loss for water utilities. Future work will address the study of the effectiveness of the proposed methods in larger WDNs. In addition, an interesting direction would be to explore an active leakage detection approach, where the pressure is deliberately increased during night hours to increase the detectability of leakages using the proposed methodology, considering a trade-off between detectability and energy/water loss.

References

[1] B. Kingdom, R. Liemberger, and P. Marin, "The challenge of reducing non-revenue water (NRW) in developing countries—How the private sector can help: A look at performance-based service contracting," World Bank, Washington, DC, USA, WSS Sector Board Discuss. Paper 8, Dec. 2006.

[2] S. G. Vrachimis, D. G. Eliades, and M. M. Polycarpou, "Real-time hydraulic interval state estimation for water transport networks: A case study," *Drinking Water Eng. Sci.*, vol. 11, no. 1, pp. 19–24, Mar. 2018.

[3] S. Díaz, R. Mínguez, and J. González, "Topological observability analysis in water distribution systems," *J. Water Resour. Planning Manage.*, vol. 143, no. 5, May 2017, Art. no. 06017001.

[4] A. Alawadhi and D. M. Tartakovsky, "Bayesian update and method of distributions: Application to leak detection in transmission mains," *Water Resour. Res.*, vol. 56, no. 2, Feb. 2020, Art. no. e2019WR025879.

[5] X. Wang *et al.*, "Pipeline leak localization using matched-field processing incorporating prior information of modeling error," *Mech. Syst. Signal Process.*, vol. 143, Sep. 2020, Art. no. 106849.

[6] S. Meniconi *et al.*, "Anomaly pre-localization in distribution–transmission mains by pump trip: Preliminary field tests in the Milan pipe system," *J. Hydroinform.*, vol. 17, no. 3, pp. 377–389, May 2015.

[7] N. Avni, B. Fishbain, and U. Shamir, "Water consumption patterns as a basis for water demand modeling," *Water Resour. Res.*, vol. 51, no. 10, pp. 8165–8181, Oct. 2015.

[8] C. T. Arsene, D. Al-Dabass, and J. Hartley, "Confidence limit analysis of water distribution systems based on a least squares loop flows state estimation technique," in *Proc. 5th Eur. Symp. Comput. Modeling Simulation (UKSim)*, 2011, pp. 94–101.

[9] S. Díaz, R. Mínguez, J. González, and D. Savic, "Explicit expressions for state estimation sensitivity analysis in water systems," *J. Water Resour. Planning Manage.*, vol. 144, no. 4, Apr. 2018, Art. no. 06018001.

[10] P. F. Boulos, K. E. Lansey, and B. W. Karney, *Comprehensive Water Distribution Systems Analysis Handbook for Engineers and Planners*. Pasadena, CA, USA: MWH Soft, 2006.

[11] A. K. Nagar and R. S. Powell, "Observability analysis of water distribution systems under parametric and measurement uncertainty," in *Proc. Building Partnerships*. Reston, VA, USA: ASCE, Sep. 2000, pp. 1–10.

[12] S. Díaz, J. González, and R. Mínguez, "Uncertainty evaluation for constrained state estimation in water distribution systems," *J. Water Resour. Planning Manage.*, vol. 142, no. 12, Dec. 2016, Art. no. 06016004.

[13] D. Kang and K. Lansey, "Real-time optimal valve operation and booster disinfection for water quality in water distribution systems," *J. Water Resour. Planning Manage.*, vol. 136, no. 4, pp. 463–473, Jul. 2010.

[14] A. Bargiela, W. Pedrycz, and M. Tanaka, "A study of uncertain state estimation," *IEEE Trans. Syst., Man, Cybern. A, Syst. Humans*, vol. 33, no. 3, pp. 288–301, May 2003.

[15] S. G. Vrachimis, S. Timotheou, D. G. Eliades, and M. M. Polycarpou, "Iterative hydraulic interval state estimation for water distribution networks," *J. Water Resour. Planning Manage.*, vol. 145, no. 1, Jan. 2019, Art. no. 04018087.

[16] A. Bargiela and G. D. Hainsworth, "Pressure and flow uncertainty in water systems," *J. Water Resour. Planning Manage.*, vol. 115, no. 2, pp. 212–229, 1989.

[17] D. G. Eliades, D. Stavrou, S. G. Vrachimis, C. G. Panayiotou, and M. M. Polycarpou, "Contamination event detection using multi-level thresholds," *Proc. Eng.*, vol. 119, pp. 1429–1438, 2015.

[18] D. Efimov, W. Perruquetti, T. Raissi, and A. Zolghadri, "Interval observers for time-varying discrete-time systems," *IEEE Trans. Autom. Control*, vol. 58, no. 12, pp. 3218–3224, Dec. 2013.

[19] Y. Wang, D. M. Bevly, and R. Rajamani, "Interval observer design for LPV systems with parametric uncertainty," *Automatica*, vol. 60, pp. 79–85, Oct. 2015.

[20] T. Raïssi, D. Efimov, and A. Zolghadri, "Interval state estimation for a class of nonlinear systems," *IEEE Trans. Autom. Control*, vol. 57, no. 1, pp. 260–265, Jan. 2012.

[21] S. G. Vrachimis, D. G. Eliades, and M. M. Polycarpou, "Leak detection in water distribution systems using hydraulic interval state estimation," in *Proc. IEEE Conf. Control Technol. Appl. (CCTA)*, Aug. 2018, pp. 565–570.

[22] W. Kühn, "Rigorously computed orbits of dynamical systems without the wrapping effect," *Computing*, vol. 61, no. 1, pp. 47–67, 1998.

[23] T. Alamo, J. M. Bravo, and E. F. Camacho, "Guaranteed state estimation by zonotopes," *Automatica*, vol. 41, no. 6, pp. 1035–1043, 2005.

[24] J. M. Bravo, T. Alamo, and E. F. Camacho, "Bounded error identification of systems with time-varying parameters," *IEEE Trans. Autom. Control*, vol. 51, no. 7, pp. 1144–1150, Jul. 2006.

[25] M. Althoff, O. Stursberg, and M. Buss, "Reachability analysis of nonlinear systems with uncertain parameters using conservative linearization," in *Proc. 47th IEEE Conf. Decis. Control*, Dec. 2008, pp. 4042–4048.

[26] C. Combastel, "Merging Kalman filtering and zonotopic state bounding for robust fault detection under noisy environment," in *Proc. 9th IFAC Symp. Fault Detection, Supervis. Saf. Tech. Processes*, 2015, pp. 289–295.

[27] J. K. Scott, R. Findeisen, R. D. Braatz, and D. M. Raimondo, "Input design for guaranteed fault diagnosis using zonotopes," *Automatica*, vol. 50, no. 6, pp. 1580–1589, Jun. 2014.

[28] F. Xu, V. Puig, C. Ocampo-Martinez, S. Olaru, and S.-I. Niculescu, "Robust MPC for actuator-fault tolerance using set-based passive fault detection and active fault isolation," *Int. J. Appl. Math. Comput. Sci.*, vol. 27, no. 1, pp. 43–61, 2017.

[29] Y. Wang, V. Puig, and G. Cembrano, "Set-membership approach and Kalman observer based on zonotopes for discrete-time descriptor systems," *Automatica*, vol. 93, pp. 435–443, Jul. 2018.

[30] J. Blesa, V. Puig, J. Saludes, and J. Vento, "Leak detection, isolation and estimation in pressurized water pipe networks using LPV models and zonotopes," in *Proc. 8th IFAC Symp. Nonlinear Control Syst.*, 2010, pp. 36–41.

[31] P. Cugueró-Escofet, J. Blesa, R. Pérez, M. A. Cuguero-Escofet, and G. Sanz, "Assessment of a leak localization algorithm in water networks under demand uncertainty," in *Proc. 9th IFAC Symp. Fault Detection, Supervis. Saf. Tech. Processes*, 2015, pp. 226–231.

[32] M. Althoff, O. Stursberg, and M. Buss, "Computing reachable sets of hybrid systems using a combination of zonotopes and polytopes," *Nonlinear Anal., Hybrid Syst.*, vol. 4, no. 2, pp. 233–249, 2010.

[33] J. K. Scott, D. M. Raimondo, G. R. Marseglia, and R. D. Braatz, "Constrained zonotopes: A new tool for set-based estimation and fault detection," *Automatica*, vol. 69, pp. 126–136, Jul. 2016.

[34] B. S. Rego, D. M. Raimondo, and G. V. Raffo, "Set-based state estimation of nonlinear systems using constrained zonotopes and interval arithmetic," in *Proc. Eur. Control Conf. (ECC)*, Jun. 2018, pp. 1584–1589.

[35] B. S. Rego, G. V. Raffo, J. K. Scott, and D. M. Raimondo, "Guaranteed methods based on constrained zonotopes for set-valued state estimation of nonlinear discrete-time systems," *Automatica*, vol. 111, Jan. 2020, Art. no. 108614.

[36] D. M. Raimondo, G. R. Marseglia, R. D. Braatz, and J. K. Scott, "Closed-loop input design for guaranteed fault diagnosis using set-valued observers," *Automatica*, vol. 74, pp. 107–117, Dec. 2016.

[37] R. E. Moore, R. B. Kearfott, and M. J. Cloud, *Introduction to Interval Analysis*. Philadelphia, PA, USA: SIAM, 2009.

[38] J. A. Kelner and D. A. Spielman, "A randomized polynomial-time simplex algorithm for linear programming," in *Proc. 38th Annu. ACM Symp. Theory Comput.*, 2006, pp. 51–60.

[39] V. T. H. Le, C. Stoica, T. Alamo, and E. F. Camacho, "Zonotopic guaranteed state estimation for uncertain systems," *Automatica*, vol. 49, no. 11, pp. 3418–3424, Nov. 2013.

[40] W. Hagemann, "Efficient geometric operations on convex polyhedra, with an application to reachability analysis of hybrid systems," *Math. Comput. Sci.*, vol. 9, no. 3, pp. 283–325, Oct. 2015.

[41] A. Neumaier, *Interval Methods for Systems of Equations*. Cambridge, U.K.: Cambridge Univ. Press, 1990.
[42] B. Greyvenstein and J. E. van Zyl, "An experimental investigation into the pressure-leakage relationship of some failed water pipes," *J. Water Supply, Res. Technol.-Aqua*, vol. 56, no. 2, pp. 117–124, Mar. 2007.
[43] S. Mohapatra, A. Sargaonkar, and P. K. Labhasetwar, "Distribution network assessment using EPANET for intermittent and continuous water supply," *Water Resour. Manage.*, vol. 28, no. 11, pp. 3745–3759, Sep. 2014.
[44] A. Zanfei, A. Menapace, S. Santopietro, and M. Righetti, "Calibration procedure for water distribution systems: Comparison among hydraulic models," *Water*, vol. 12, no. 5, p. 1421, May 2020.
[45] J. H. Andersen, R. S. Powell, and J. F. Marsh, "Constrained state estimation with applications in water distribution network monitoring," *Int. J. Syst. Sci.*, vol. 32, no. 6, pp. 807–816, Jan. 2001.
[46] C. Battisti. (May 29, 2021). *Pressure Transmitter for Industrial Applications-Piezoresistive Sensor*. [Online]. Available: https://www.nuovafima.com/en/prodotti/st-9-en
[47] R. Guercio, R. Magini, and I. Pallavicini, "Instantaneous residential water demand as stochastic point process," *Trans. Ecol. Environ.*, vol. 48, pp. 1–10, Jan. 2001.
[48] M. Xenochristou, C. Hutton, J. Hofman, and Z. Kapelan, "Short-term forecasting of household water demand in the UK using an interpretable machine learning approach," *J. Water Resour. Planning Manage.*, vol. 147, no. 4, Apr. 2021, Art. no. 04021004.
[49] G. Guo, S. Liu, Y. Wu, J. Li, R. Zhou, and X. Zhu, "Short-term water demand forecast based on deep learning method," *J. Water Resour. Planning Manage.*, vol. 144, no. 12, Dec. 2018, Art. no. 04018076.
[50] L. A. Rossman, "EPANET 2: Users manual," US Environ. Protection Agency, Cincinnati, OH, USA, Tech. Rep. EPA/600/R–00/057, 2000.
[51] X. Yang and J. K. Scott, "A comparison of zonotope order reduction techniques," *Automatica*, vol. 95, pp. 378–384, Sep. 2018.
[52] L. Chisci, A. Garulli, and G. Zappa, "Recursive state bounding by parallelotopes," *Automatica*, vol. 32, no. 7, pp. 1049–1055, Jul. 1996.
[53] S. G. Vrachimis, R. Lifshitz, D. G. Eliades, M. M. Polycarpou, and A. Ostfeld, "Active contamination detection in water-distribution systems," *J. Water Resour. Planning Manage.*, vol. 146, no. 4, Apr. 2020, Art. no. 04020014.
[54] M. Casillas, V. Puig, L. Garza-Castanón, and A. Rosich, "Optimal sensor placement for leak location in water distribution networks using genetic algorithms," *Sensors*, vol. 13, no. 11, pp. 14984–15005, 2013.

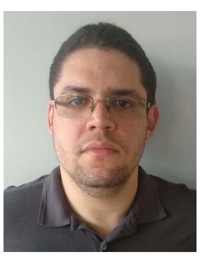

Brenner S. Rego received the B.S. degree in electrical engineering from the Federal University of Goiás, Goiânia, Brazil, in 2014, and the M.S. and Ph.D. degrees in electrical engineering from the Federal University of Minas Gerais, Belo Horizonte, Brazil, in 2016 and 2021, respectively.

He is currently a Post-Doctoral Fellow in electrical engineering with the Federal University of Minas Gerais. He is the author or coauthor of diverse papers published in refereed journals and conference proceedings. From September 2019 to June 2020, he was a Visiting Ph.D. Student at the University of Pavia, Pavia, Italy. His current research interests include set-based state estimation, active fault diagnosis and fault-tolerant control, modeling and control of unmanned aerial vehicles, and aerial load transportation.

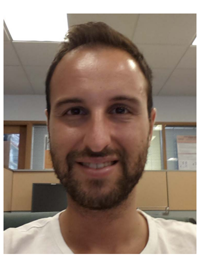

Stelios G. Vrachimis (Member, IEEE) received the B.Sc. and Ph.D. degrees in electrical engineering from the Department of Electrical and Computer Engineering, University of Cyprus, Nicosia, Cyprus, in 2011 and 2020, respectively, and the M.Sc. degree in control systems from Imperial College London, London, U.K., in 2012.

From 2012 to 2020, he was a graduate-level Researcher at the KIOS Research and Innovation Center of Excellence, University of Cyprus, where he is currently a Post-Doctoral Research Associate. His research interests include the optimization, real-time state estimation, fault-diagnosis, and fault-adaptive control of critical infrastructure systems, with applications focused on water distribution systems.

Dr. Vrachimis is a member of the Cyprus Technical Chamber and Cyprus Young Water Professionals. He has volunteered as a reviewer to IEEE transactions and conferences and has served as an Associate Editor for the *Journal of Water Resources Planning and Management*.

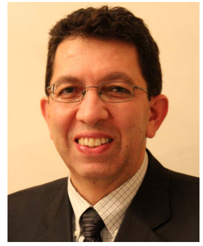

Marios M. Polycarpou (Fellow, IEEE) received the B.A. degree in computer science and the B.Sc. degree in electrical engineering from Rice University, Houston, TX, USA, in 1987, and the M.S. and Ph.D. degrees in electrical engineering from the University of Southern California, Los Angeles, CA, USA, in 1989 and 1992, respectively.

He is currently a Professor of electrical and computer engineering and the Director of the KIOS Research and Innovation Center of Excellence, University of Cyprus, Nicosia, Cyprus. He is also a member of the Cyprus Academy of Sciences, Letters, and Arts, and an Honorary Professor of Imperial College London, London, U.K. He has published more than 400 articles in refereed journals, edited books, and refereed conference proceedings and coauthored seven books. He also holds six patents. His teaching and research interests are in intelligent systems and networks, adaptive and learning control systems, fault diagnosis, machine learning, and critical infrastructure systems.

Prof. Polycarpou is a fellow of the IFAC. He received the 2016 IEEE Neural Networks Pioneer Award. He was a recipient of the 2014 Best Paper Award for the journal *Building and Environment* (Elsevier). He served as the President of the IEEE Computational Intelligence Society (2012–2013), as the President of the European Control Association (2017–2019), and as the Editor-in-Chief of the IEEE TRANSACTIONS ON NEURAL NETWORKS AND LEARNING SYSTEMS (2004–2010). He serves on the Editorial Boards of the PROCEEDINGS OF THE IEEE, the *Annual Reviews in Control*, and the *Foundations and Trends in Systems and Control*. His research work has been funded by several agencies and industry in Europe and the United States, including the prestigious European Research Council (ERC) Advanced Grant, the ERC Synergy Grant, and the EU Teaming Project.

Guilherme V. Raffo was born in Porto Alegre, Brazil. He received the B.Sc. degree in automation and control engineering from the Pontifical Catholic University of Rio Grande do Sul, Porto Alegre, in 2002, the Specialist degree in industrial automation from the Federal University of Rio Grande do Sul, Porto Alegre, in 2003, the M.Sc. degree in electrical engineering from the Federal University of Santa Catarina, Florianópolis, Brazil, in 2005, the M.Sc. degree in automation, robotics, and telematics, and the Ph.D. degree from the University of Seville, Seville, Spain, in 2007 and 2011, respectively.

From 2011 to 2012, he was a Post-Doctoral Fellow with the Federal University of Santa Catarina. He is currently an Associate Professor with the Federal University of Minas Gerais, Belo Horizonte, Brazil. He is the author or coauthor of more than 90 publications, including journal articles, book chapters, and conference proceedings. His current research interests include robust control, nonlinear control, H-control theory, predictive control, set-membership state estimation, fault-tolerant control, unmanned aerial vehicles, robotics, and underactuated systems.

Davide M. Raimondo (Member, IEEE) received the Ph.D. degree in electronics, computer science, and electrical engineering from the University of Pavia, Pavia, Italy, in 2009.

From 2009 to 2010, he was a Post-Doctoral Fellow with the Automatic Control Laboratory, ETH Zürich, Zürich, Switzerland. From 2010 to 2015 and from 2015 to 2021, he was an Assistant Professor and Associate Professor with the University of Pavia, respectively, where he will hold the position of Full Professor in December 2021. He has held visiting positions at MIT, Cambridge, MA, USA; the University of Seville, Seville, Spain; TU Wien, Vienna, Austria; and the University of Konstanz, Konstanz, Germany. He is the author or coauthor of more than 100 papers published in refereed journals, books, and conference proceedings. His current research interests include battery management systems, set-based estimation, fault diagnosis, fault-tolerant control, model predictive control, and optimization.

Prof. Raimondo, with coauthors, received the 2014–2016 Automatica Paper Prize Award in 2017. He serves as a Subject Editor for *Automatica* and IEEE TRANSACTIONS ON CONTROL SYSTEMS TECHNOLOGY.